Mon. Not. R. Astron. Soc. **000**, 1–21 (2007) Printed 21 February 2013 (MN LaTeX style file v2.2)

The stellar association around Gamma Velorum and its relationship with Vela OB2

R.D. Jeffries[1], Tim Naylor[2], F.M. Walter[3], M.P. Pozzo[4] and C.R. Devey[1]
[1] *Astrophysics Group, Research Institute for the Environment, Physical Sciences and Applied Mathematics, Keele University, Keele, Staffordshire ST5 5BG*
[2] *School of Physics, University of Exeter, Stocker Road, Exeter EX4 4QL*
[3] *Department of Physics and Astronomy, State University of New York, Stony Brook, NY 11794-3800, USA*
[4] *Department of Earth Sciences and Materials Simulation Laboratory, University College London, Gower Street, London WC1E 6BT*

Submitted September 2008

ABSTRACT

We present the results of a photometric BVI survey of 0.9 square degrees around the Wolf-Rayet binary γ^2 Vel and its early-type common proper motion companion γ^1 Vel (together referred to as the γ Vel system). Several hundred pre-main-sequence (PMS) stars are identified and the youth of a subset of these is spectroscopically confirmed by the presence of lithium in their atmospheres, Hα emission and high levels of X-ray activity. We show that the PMS stars are kinematically coherent and spatially concentrated around γ Vel. The PMS stars have similar proper motions to γ Vel, to main-sequence stars around γ Vel and to early-type stars of the wider Vela OB2 association of which γ^2 Vel is the brightest member. The ratio of main-sequence stars to low-mass (0.1–0.6 $M_\odot$) PMS stars is consistent with a Kroupa (2001) mass function. Main-sequence fitting to stars around γ Vel gives an association distance modulus of 7.76 ± 0.07 mag, which is consistent with a similarly-determined distance for Vela OB2 and also with interferometric distances to γ^2 Vel. High-mass stellar models indicate an age of 3–4 Myr for γ^2 Vel, but the low-mass PMS stars have ages of $\simeq$ 10 Myr according to low-mass evolutionary models and 5–10 Myr by empirically placing them in an age sequence with other clusters based on colour-magnitude diagrams and lithium depletion. We conclude that the low-mass PMS stars form a genuine association with γ Vel and that this is a subcluster within the larger Vela OB2 association. We speculate that γ^2 Vel formed after the bulk of the low-mass stars, expelling gas, terminating star formation and unbinding the association. The velocity dispersion of the PMS stars is too low for this star forming event to have produced all the stars in the extended Vela OB2 association. Instead, star formation must have been initiated at several sites within a molecular cloud, either sequentially or, simultaneously after some triggering event.

Key words: stars: formation – stars: pre-main-sequence – stars: Wolf-Rayet – open clusters and associations: Vela OB2

1 INTRODUCTION

The double lined spectroscopic binary system γ^2 Vel (HD 68273) contains the closest example of a Wolf-Rayet star. The two components of the binary orbit with a period of 78.5 days and have spectral types WC8 (Smith 1968) and O8III (Schaerer, Schmutz & Grenon 1997). Although the Hipparcos parallax to the system yields a distance of only 258^{+41}_{-31} pc, de Zeeuw et al. (1999) classify it as belonging to the Vela OB2 association, a group of some 100 early-type stars spread over an angular diameter of $\sim 10^\circ$ and at a mean distance of 410 ± 12 pc. Indeed, the distance to γ^2 Vel is somewhat controversial. Millour et al. (2007) found an interferometric distance of 368^{+38}_{-13} pc, while North et al. (2007) have combined interferometry with radial velocity measurements to estimate a distance of 336^{+8}_{-7} pc. A revised analysis of the Hipparcos data by van Leeuwen (2007) quotes a distance of 334^{+40}_{-32} pc. A further common proper-motion component of the system, γ^1 Vel (HD 68243), lies 41 arcseconds to the south-west of γ^2 Vel. It is an SB1 binary with a B2III primary and a period of 1.48 days (Hernández & Sahade 1980). The system formed by γ^1 and γ^2 Vel will hereafter be referred to as γ Vel.

Pozzo et al. (2000) presented results of *ROSAT* X-ray

observations combined with a photometric survey in a region surrounding γ Vel. A large number of X-ray sources were found coinciding with low-mass stars that were identified with a few Myr pre-main-sequence (PMS) isochrone at a distance of 350–450 pc. Pozzo et al. argued that these low-mass stars were physically associated with γ Vel and that they are all part of the Vela OB2 association.

In this paper we present a BVI photometric survey of about 0.9 square degrees around γ Vel which is complete to $V \sim 20$. This area is more extended than that considered by Pozzo et al. (2000) and allows us to revisit the question of the spatial distribution of the low-mass association. We present optical spectroscopy of a subsample of the PMS candidates which confirms both the youth and kinematic coherence of the association. We have also used *XMM-Newton* observations around γ Vel to examine the X-ray properties of the low-mass PMS candidates and define a secure sample of association members with which to investigate their age. Finally, by combining what we have learned about the low-mass PMS stars with distances obtained from modelling upper main sequence stars around γ Vel and the age of γ Vel itself, we examine the relationship between the high- and low-mass members of this group and its place within the wider Vela OB2 association.

2 OBSERVATIONAL DATA

2.1 Optical photometry

A photometric survey of an area around γ Vel was performed at the Cerro Tololo Interamerican Observatory (CTIO) 0.9-m telescope. The survey was done in two parts in different years, but using the same instrumentation and filters, namely a Tek 2048×2048 CCD with a 13.5×13.5 arcmin^2 field of view, the Harris B and V filters and a Kron-Cousins I filter.

The first set of observations, described in Pozzo et al. (2000), consisted of eight overlapping fields surveyed on the night beginning 8 February 1999, together with five standard star fields taken from the Landolt (1992) catalogue. Both short (20, 10, 6s) and long (300, 120, 60s) exposures were taken through the B, V, I filters at each of the field centres listed in Table 1. The data were taken in photometric conditions.[1]

The second set of observations consisted of twenty fields which were surveyed on the nights beginning 8, 10 and 11 February 2002. These twenty fields had substantial overlap with the original eight fields and the field centres are given in Table 1. The short and long exposures also consisted of (20, 10, 6s) and (300, 120, 60s) through the B, V, I filters respectively. The data were obtained in good to photometric conditions and again observations of several Landolt (1992) fields were taken each night, some on more than one occasion. The combined 28 overlapping fields make a survey of roughly constant sensitivity over a rectangular area of approximately 0.93×0.95 degrees, centred upon γ^2 Vel.

[1] The exposure times of (20, 10, 10s) and (200, 100, 100s) previously stated by Pozzo et al. (2000) were incorrect, but this error was not present in the calculated magnitudes in that paper.

Table 1. A log of the observations used in this work. For each of the fields below, we obtained exposures of (300, 20s), (120, 10s) and (60, 6s) through the B, V and I filters respectively.

Field	Date	Field Centre (J2000) RA	Dec
01	1999-02-09	08 10 17	-47 20 29
02	1999-02-09	08 09 36	-47 13 32
03	1999-02-09	08 08 52	-47 20 39
04	1999-02-09	08 09 32	-47 27 48
05	1999-02-09	08 10 35	-47 09 47
06	1999-02-09	08 08 24	-47 09 44
07	1999-02-09	08 08 24	-47 31 42
08	1999-02-09	08 10 34	-47 31 38
09	2002-02-09	08 09 31	-47 09 24
10	2002-02-09	08 10 26	-47 20 23
11	2002-02-09	08 09 31	-47 31 24
12	2002-02-09	08 08 26	-47 20 23
13	2002-02-12	08 07 22	-47 41 42
14	2002-02-12	08 07 22	-47 31 22
15	2002-02-11	08 07 22	-47 20 23
16	2002-02-11	08 07 22	-47 09 22
17	2002-02-11	08 07 22	-46 58 23
18	2002-02-11	08 08 26	-46 58 21
19	2002-02-11	08 09 31	-46 58 22
20	2002-02-11	08 10 26	-46 58 23
21	2002-02-11	08 11 30	-46 58 23
22	2002-02-11	08 11 30	-47 09 23
23	2002-02-11	08 11 30	-47 20 23
24	2002-02-12	08 11 30	-47 31 24
25	2002-02-12	08 11 30	-47 41 24
26	2002-02-12	08 10 26	-47 41 22
27	2002-02-12	08 09 31	-47 41 23
28	2002-02-12	08 08 26	-47 41 22

The data were initially reduced by subtracting a median stacked bias frame and overscan and then normalising with flat fields taken during twilight sky on each night. A bad pixel mask was constructed to identify hot pixels and a few bad columns on the CCD. The data were analysed using the CLUSTER software package described by Naylor et al. (2002), with updates described in Burningham et al. (2003) and Jeffries et al. (2004). Objects were identified in the long V-band exposures (or short V exposures if saturated in the long). Spatial transformations were calculated between the separate exposures for each field and optimal photometry (Naylor 1998) was performed to obtain a flux for each object in each exposure at a given position. A spatially varying "profile correction" was calculated from bright, unsaturated stars in each frame so that the photometry could later be calibrated with standard star observations. The profile-corrected photometry in each band was combined in a weighted fashion after adjustments were made for any airmass difference. An additional statistical uncertainty was added to each measurement at this stage to ensure that a plot of signal-to-noise versus chi-squared for the combined measurements was flat and approximately equal to unity (see Naylor et al. 2002 for details). This additional uncertainty ranged from 0.007 to 0.015 mag for the 28 fields and reflects uncertainties in the profile correction. Astrometric calibration of each frame was performed using the positions of 600–900 stars from the 2MASS point source catalogue

(Cutri et al. 2003). The rms residuals were approximately 0.08 arcseconds in each coordinate.

Standard star magnitudes were measured through a 15 pixel (6 arcsec) radius aperture and weighted least squares solutions to the following equations were found for each night.

$$B-V = \psi_{bv}\,(b-v) - k_{bv}X + z_{bv}\,, \quad (1)$$

$$V-I = \psi_{vi}\,(v-i) - k_{vi}X + z_{vi}\,, \quad (2)$$

$$V = v + \psi_{v}\,(B-V) - k_{v}X + z_{v}\,, \quad (3)$$

where b, v, i are the instrumental magnitudes, X is the airmass, k are the extinction coefficients, z the zeropoints and ψ are the colour terms. Standard stars were measured with a range of colours, but included only two with $V-I > 2.5$ (the reddest had $V-I = 5.8$). The means of the colour terms were found to be $\psi_{bv} = 0.89$, $\psi_{vi} = 1.00$ and $\psi_{v} = 0.02$, indicating that the filter set used was close to the natural Johnson-Kron-Cousins system defined by the standards. Using these transformations the magnitudes were place onto the Johnson-Kron-Cousins BVI system. The last step in the construction of the catalogue was to make the photometric calibration uniform across the mosaic using stars in the overlapping regions of each frame (see Jeffries et al. 2004). The adjustments made here were generally less than 0.02 mag and the remaining rms differences for stars in the overlap regions was about 0.01 mag in V, $B-V$ and $V-I$.

The final optical catalogue is presented in Table 2 (available fully in electronic form only). The flags applied to the photometric values (non-stellar, bad sky, saturation etc.) are detailed in Burningham et al. (2003). Some of these flags, particularly the ill-determined background (flagged "I"), are quite conservative but this ensures that the unflagged stars have photometry of very high quality. The final photometric uncertainties listed in the catalogue include the additional systematic error associated with the profile correction but do not include the 0.01 mag rms found for stars in the overlapping field regions. This additional error should be added when comparing or combining stars across different fields or the whole survey (as in this paper). Finally there are likely to be external systematic photometric uncertainties associated with placing our photometry onto the standard system. The residuals of the fits to the standard star magnitudes suggest that any uncertainties are limited to less than 0.02 mag in the reported magnitudes and colours for stars with $V-I \leqslant 2.5$. This may rise for redder stars where there is a paucity of available photometric standards.

The final colour-magnitude diagrams (CMDs) are shown in Fig. 1 for unflagged stars with statistical uncertainties of less than 0.1 mag on each axis. The PMS identified by Pozzo et al. (2000) is readily appearent, especially in the V vs $V-I$ CMD where for $V-I > 1.6$ it stands well clear of contamination. In the V vs $B-V$ CMD there appear to be some very faint blue objects. Upon visual inspection most of these appear to be situated along the diffraction spikes of bright, presumably early-type stars, but the detections were too faint for them to be correctly identified as non-stellar.

A histogram of V magnitudes suggests that the V vs $V-I$ CMD is almost complete to $V = 20$ for colours and magnitudes with uncertainties < 0.1 mag. The catalogue is "almost" complete to this level because there are instances where brighter stars are flagged as non-stellar or have a bad or ill-determined sky flag. This is especially true in a 3 arcminute radius immediately around γ Vel itself, where almost every star is saturated or has photometry affected by scattered light from γ Vel, but is also the case for much smaller regions around other bright stars in the survey area. The completeness at the bright end is governed by the saturation level in the short exposures which is at about $V = 10.5$ mag, with small variations across the mosaic. Excluding the central 3 arcminute radius, 86 per cent of stars with $11 < V < 20$ have unflagged photometry and photometric uncertainties of < 0.1 mag. This fraction is not very magnitude dependent, falling from $\simeq 93$ per cent for $V < 16$ to 83 per cent for $19 < V < 20$.

2.2 Optical Spectroscopy

On 24 and 25 November 1999 we used the 4-m Blanco telescope at CTIO in conjunction with the Hydra multi-fibre spectrograph to obtain high resolution ($R \simeq 25000$) spectra of 120 candidate members of the low-mass association around γ Vel. Targets were selected from the original photometric survey discussed in Pozzo et al. (2000) (the eight fields observed in February 1999) and so come from the central ~ 0.3 square degrees of our total optical survey. Targets were chosen solely on the basis of their position in the V vs $V-I$ CMD.

The 31.6 l/mm echelle grating and filter #5 were used to isolate order 8, achieving a wavelength coverage from about 6450Å to 6750Å. The detector was a Loral 3k with 15 micron pixels. We operated at gain setting 4, which yields about 2 electrons per ADU and 7.5 electrons of read noise per pixel.

The same field centre was observed twice on successive nights, observing mainly different stars on each occasion. There were 70 fibres in use at the time of our observations. We observed 62 and 58 targets in the two observations with 3×600s exposures. A few targets were included in both configurations, so a total of 112 separate targets were observed. Sky spectra were obtained through 7 and 6 fibres, respectively, on the two nights. Not all fibres were used because of targeting constraints. Spectra of the daylight sky were used to establish fibre throughputs - with two exceptions they vary by less than a factor of 2, although two fibers had a very low throughput. One or two stars were abnormally faint (for their magnitude) in each field. We attribute this to mispositioning of the fibre.

A Th-Ar calibration lamp was observed at the start and end of the night to establish the dispersion solution. An etalon lamp was observed before and after each observation to track shifts in the zero-point of the wavelength solution. The data were flattened using dome flats illuminated by a quartz lamp.

Data reductions and extractions were accomplished using standard IRAF tasks including the extraction of 1-dimensional spectra and application of the dispersion solution. A scattered light correction was applied. The twilight sky was observed each night to establish the zero point of the radial velocities. Some examples of the spectra are shown in Fig. 2.

Radial velocities (RVs) were measured by cross-correlating the spectra against those of the sky taken through the same fibre. The statistical uncertainties are estimated to be about 2–3 $\mathrm{km\,s^{-1}}$ for the reported RVs,

Table 2. The photometric catalogue for a 0.9 square degree area around γ Vel. Only a few rows are shown here to illustrate the content, the full table is available in electronic form. The columns list two identifying numbers (the first of which is the field number from Table 1), the RA and Dec (J2000), an x,y pixel position on the CCD where the object was identified and then for each of V, $B-V$ and $V-I$ there is a magnitude, uncertainty and a quality flag. The flagging system is described in detail by Burningham et al. (2003).

Identifier		RA	Dec	x	y	V			$B-V$			$V-I$		
14	6058	08 06 38.742	-47 37 17.96	2057.835	1900.018	21.483	0.680	EN	2.936	0.898	EN	1.789	0.868	NN
14	413	08 06 38.756	-47 33 56.51	2058.757	1398.062	17.033	0.029	EO	6.987	0.667	EO	0.878	0.028	OO
14	1571	08 06 38.756	-47 34 46.17	2058.448	1521.786	18.915	0.025	EO	5.285	0.667	EO	1.883	0.070	OO
14	4261	08 06 38.787	-47 36 03.27	2057.166	1713.902	20.921	0.098	EO	3.462	0.672	EO	1.337	0.159	OO
14	1040	08 06 38.838	-47 35 43.23	2056.024	1663.976	18.323	0.016	OO	0.723	0.021	OO	0.889	0.029	OO
						...								

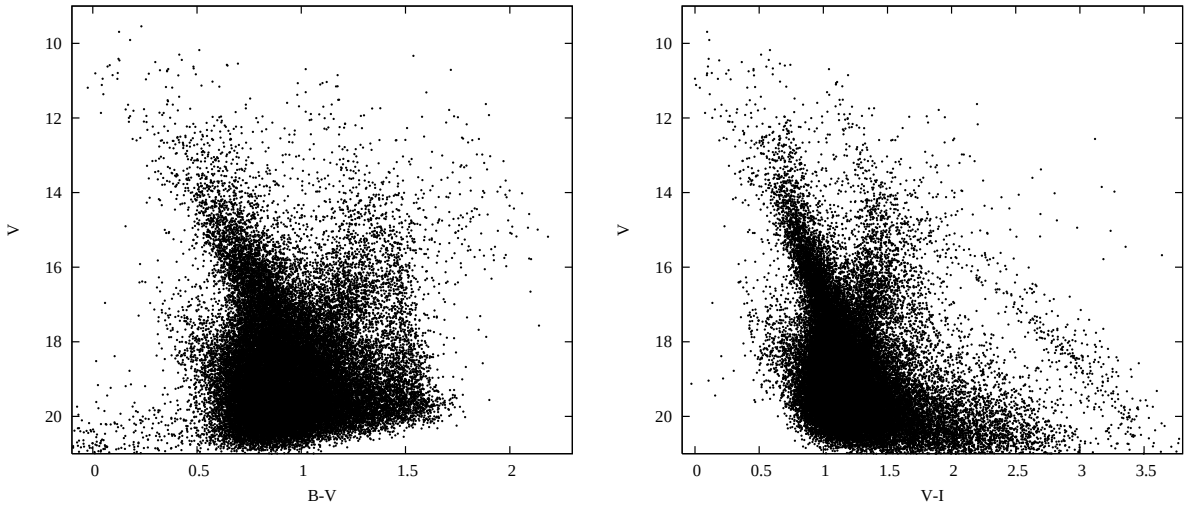

Figure 1. Colour-magnitude diagrams (CMDs) from the entire survey area. Only unflagged photometric points with uncertainties less than 0.1 mag in each coordinate are plotted – 38345 stars for the V, $B-V$ diagram and 40185 stars for the V, $V-I$ diagram. A clear PMS stands out in the V versus $V-I$ CMD for $V-I>1.6$.

Table 3. Spectroscopy results. Only a few rows are shown here to illustrate the content. The full table is available in electronic form. Column 1 lists which night the spectra were obtained: 1 = 24 November 1999, 2 = 25 November 1999. Columns 2 and 3 give the source identification number (as in Table 2). Columns 4–14 (omitted from the table sample shown below, but included for convenience in the electronic version) repeats the Table 2 values of RA, Dec (J2000) and the photometry values, uncertainties and flags for these sources. Column 15 gives the signal-to-noise ratio per pixel for the spectrum estimated from the continuum around the Li I line. Columns 16 and 17 give the EW and EW uncertainty for the Li I 6708Å line – a zero uncertainty indicates that the quoted W[Li] is a 2-sigma upper limit. Columns 18 and 19 give the emission EW of the Hα line – here a negative value indicates absorption. Column 20 gives the heliocentric RV measured from the spectrum. Columns 21 to 24 list the Nomad proper motions and uncertainties (in milli-arcsec/year) where available. Column 25 gives a comment based on the cross-correlation function (ccf) used to derive the RV: SB2 indicates a double peaked ccf, SB2? indicates a possible double peaked ccf, RR means the star is probably a rapid rotator (in excess of $\simeq 30\,\mathrm{km\,s^{-1}}$) and E indicates an early-type spectrum. Column 26 lists $\log(L_\mathrm{x}/L_\mathrm{bol})$ where available (see section 3.2). Column 27 gives our assessment of association membership: 1 indicates a member, 2 indicates a non-member and 3 indicates uncertain membership (see section 3.1).

(1) Night	(2)	(3) Identifier	(15) SN	(16) W[Hα] (Å)	(17) δW[Hα] (Å)	(18) W[Li] (Å)	(19) δW[Li] (Å)	(20) RV ($\mathrm{km\,s^{-1}}$)	(21) PMRa	(22) δPMRa	(23) PMDec (mas/yr)	(24) δPMDec	(25) Comment	(26) log ($L_\mathrm{x}/L_\mathrm{bol}$)	(27) Member
1	16	40	22	4.99	0.29	0.49	0.07	18	-5.7	5.6	13.4	5.6			1
1	7	35	14	-0.40	0.31	0.31	0.08	21	0.6	5.6	12.4	5.6		-2.91	1
1	6	216	5	4.3	2.2	0.43	0.15	14							1
1	9	131	6	0.52	0.56	0.50	0.13	20	-5.2	5.6	2.4	5.6		-3.45	1
2	12	123	6	0.21	0.26	0.46	0.13	30	-11.1	5.7	4.9	5.6	SB2?	-3.82	1
								...							

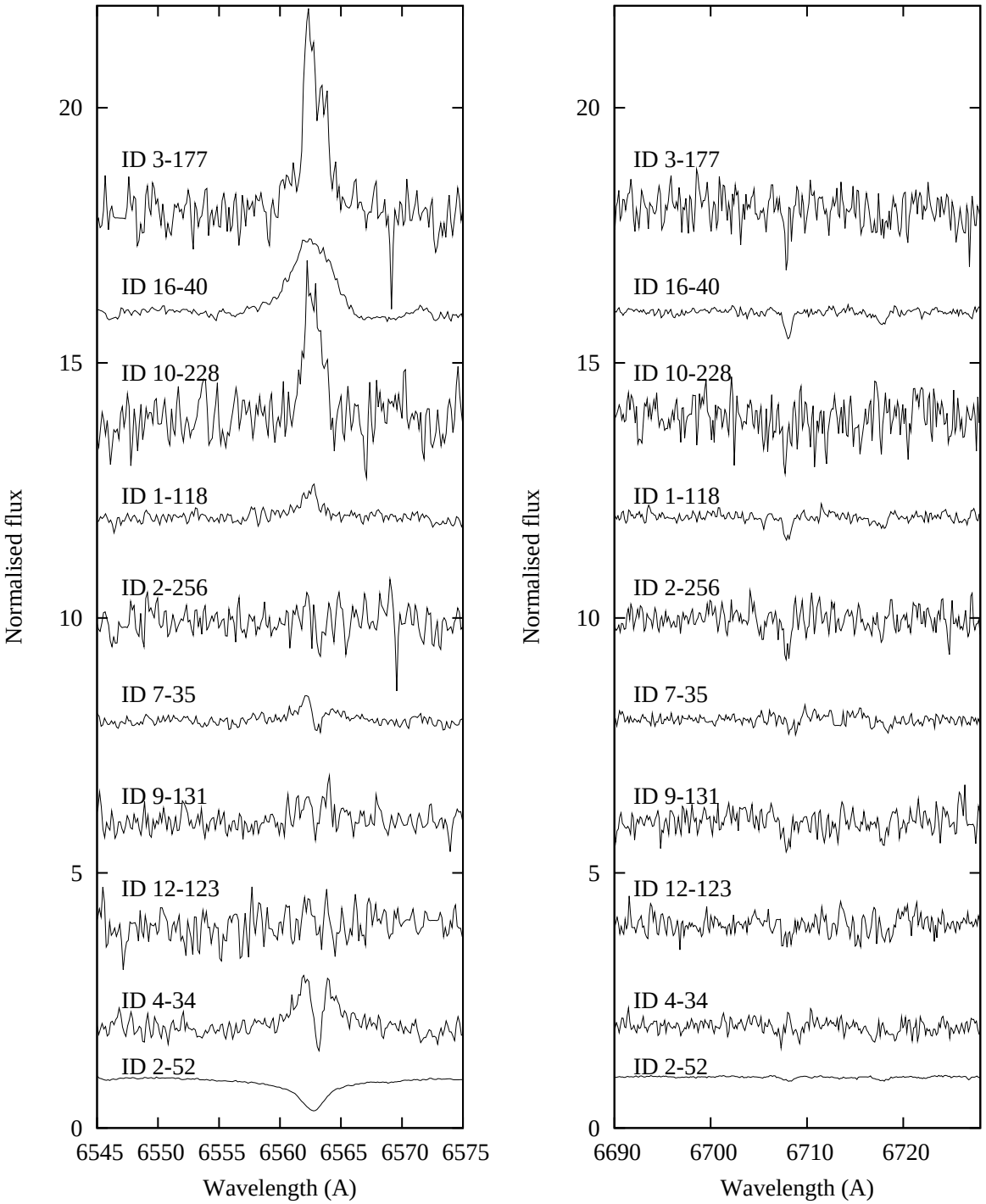

Figure 2. Examples of our spectra in the vicinities of the Hα and Li I 6708Å lines. The spectra have been normalised to unity and offset for clarity. These examples show the full diversity of signal-to-noise ratios in our sample.

although are probably worse for a few objects with the lowest signal-to-noise. In some cases no meaningful cross-correlation peak could be measured.

The equivalent widths (EWs) of the Li I 6708Å line (W[Li]) were estimated using the SPLOT task in IRAF and a continuum estimated from a clipped fit to the surrounding continuum. Estimated uncertainties are based upon the formula δW[Li]= $\sqrt{(fp)/SN}$ where f and p are the full width half maximum of the line (about 0.7Å for most objects) and the pixel size (about 0.14Å), and SN is the signal-to-noise ratio of the spectrum which is empirically estimated from the residuals to the continuum fit described above. Where the line was not significantly detected, a 2-sigma upper limit is reported.

Hα EWs were estimated in a similar way. However it should be noted that the strong Hα background signal from

the sky, as seen in the sky fibres, meant that the signal-to-noise ratio in the Hα line was usually much worse than the surrounding continuum. The EW uncertainties are dominated by errors in the fibre throughput estimates in the fainter stars. The contribution of this to the EW uncertainties was estimated using the standard deviation of the residual flux around Hα seen in the sky-subtracted spectra from fibres placed on the night sky.

The results of these analyses are presented in Table 3. In many cases, especially for spectra from the second night or for faint targets, the spectra were too poor to provide any reliable information and so Table 3 only contains results from 91 spectra of 84 individual targets. Note that seven targets have photometry flags set – indicating that their photometry cannot be considered as reliable as for the rest. The initial photometry analysis of Pozzo et al. (2000) did not flag these stars, indicating that the more stringent quality control applied here, particularly with regard to "ill-determined sky" (see section 2.1), has flagged these stars but that their photometry cannot be of very poor quality. Five of these stars are judged to be members in section 3.1 and their photometry places them squarely in the cluster pre-main-sequence. We will continue to use these stars in our analysis and in any event, their inclusion affects none of the paper's conclusions.

2.3 XMM-Newton Observations

The X-ray data used in this paper come from two observations performed in 2001 by the *XMM-Newton* satellite. The first started at at MJD 52013.473 and lasted 29.7 ks and the second began at MJD 52033.4213 and lasted 59.1 ks. The central pointing positions were close, but slightly different for each observation at RA = 122.407208 degrees, Dec = −47.358139 degrees and RA = 122.397042, Dec = −47.362889 degrees respectively. Both observations made use of the European Photon Imaging Camera (EPIC) camera with the "thick" optical filter covering the pn, m1 and m2 detectors (see Strüder et al. 2001; Turner et al. 2001).

These EPIC datasets were reduced as part of the second XMM-Newton Serendipitous Source Survey (2XMM) cataloguing effort and the positions and X-ray count rates for sources detected in these two observations were obtained from the 2XMM database (pre-release version) held at the XMM-Newton Survey Science Centre at Leicester University.

The data available consist of the positions and detection likelihoods, together with count rates determined in a number of separate energy bands and their corresponding uncertainties. For the purposes of this paper we created a merged X-ray catalogue consisting of all those sources in the longer observation plus those sources in the shorter observation with no counterpart (within 6 arcseconds) in the longer observation. Anything correlated within 6 arcseconds was assumed to be the same X-ray source – there is only a likelihood of 1 random correlation within this radius. The merged X-ray catalogue contained positions and count rates for 276 separate sources, of which just 26 were found only in the shorter observation.

3 ASSOCIATION MEMBERSHIP

3.1 Spectroscopic members

The primary basis for assigning secure membership is the optical spectroscopy, which provides two good membership indicators – the RV and strength of the Li I 6708Å feature. The RVs of association members should lie close to a uniform value, after allowing for some velocity dispersion, observational uncertainties and the possibility of close binaries. The abundance of lithium, and by extension W[Li], is an age indicator for young, cool stars (see Jeffries 2006). Lithium is depleted during the PMS phase in cool stellar envelopes leading to a decline in W[Li] at a rate which depends on the mass and hence effective temperature and colour of a star. We refrain from using Hα strength as a membership indicator because we would like to comment later on the frequency with which strong, accretion-related Hα emission is seen.

Figure 3a shows a plot of W[Li] versus RV. Where two spectra are available, the plotted information comes from the spectrum with the highest signal-to-noise ratio. This plot shows a concentration of RV values at 15–20 kms and that objects with this RV tend to have the largest values of W[Li].

Figure 3b shows W[Li] as a function of $V-I$, again plotting information from the best spectrum. The symbols are coded to indicate which targets have an RV in the range $11 \leqslant \mathrm{RV} \leqslant 22\,\mathrm{km\,s^{-1}}$. Also shown are loci defining the observed upper and lower envelopes of W[Li] as a function of $V-I$ for stars in the IC 2391, IC 2602 and NGC 2547 open clusters (Randich et al. 1997, 2001; Jeffries et al. 2003), which have ages in the range 30–50 Myr. We also show a locus appropriate for a Li abundance $A(\mathrm{Li}) = 3.1$ (where $A(\mathrm{Li}) = 12 + \log N(\mathrm{Li})/N(\mathrm{H})$), which corresponds approximately to an undepleted level of atmospheric Li. This locus was calculated using atmospheric models and colour-temperature relations described in Jeffries et al. (2003). These additional loci have been corrected by small amounts to correspond to the reddening of the γ Vel association ($E(V-I) = 0.055$, see section 4.2).

RV selection alone is unable to secure cluster membership. Fig. 3b shows that there are several stars with a "membership RV" but with a W[Li] inconsistent with being very young stars ($<$ 30 Myr). Membership or otherwise of the "γ Vel association" is assigned as follows:

(i) We consider all those stars in Fig. 3b with W[Li] above the upper empirical locus for a 30–50 Myr star to be almost certain cluster members with one exception. The star ID 6-122 is at the boundary but distinct from many other objects with $V-I \simeq 1.8$. Whilst this probably is a young star, its lack of a very large W[Li] and anomalous RV make membership of the γ Vel association doubtful.

(ii) There are five objects among the Li-rich members defined above where the RV is not in the range 11–22 $\mathrm{km\,s^{-1}}$. One of these is a clear double-lined spectroscopic binary (SB2, ID 4-34), one is a possible SB2 (ID 12-123) and for the other three (ID 1-118, ID 2-256, ID 10-228) we were unable to determine the RV because of the poor spectrum quality. The spectra of these five stars are shown in Fig. 2. On the basis of their W[Li] we consider all these to be association members.

(iii) There are eight objects with $V-I < 1.4$ that have a strong Li feature which is at or below (by less than 1.5 error

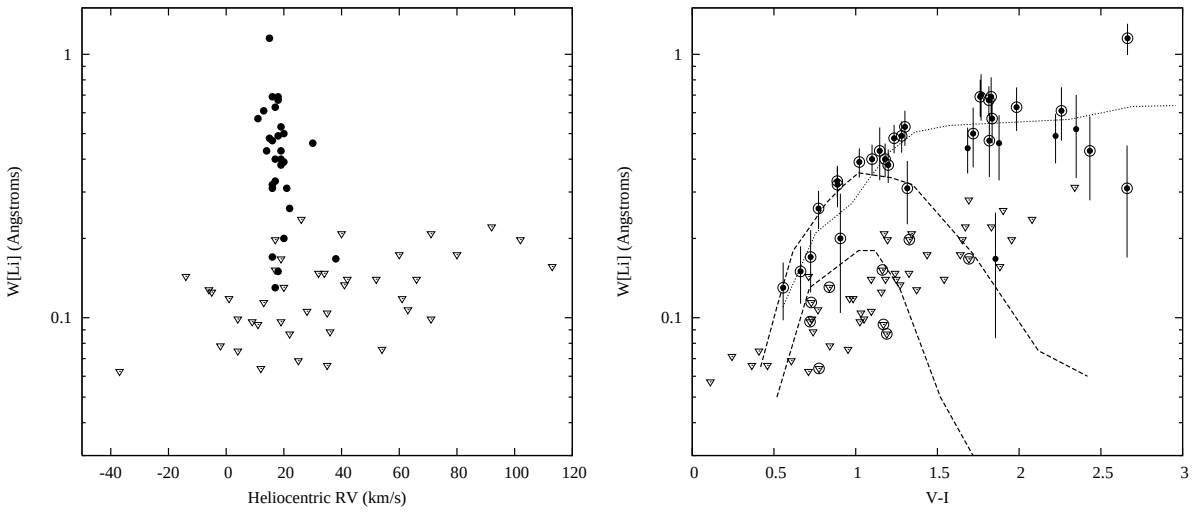

Figure 3. (a) Strength of the Li I 6708Å feature versus the heliocentric RV. The triangles represent upper limits. There is a clear concentration of objects exhibiting strong Li in a narrow range of RV. (b) Strength of the Li I 6708Å feature versus $V-I$ colour. Encircled objects have $11 \leqslant \mathrm{RV} \leqslant 22\,\mathrm{km\,s^{-1}}$. The dashed loci show observationally determined ranges of W[Li] in the 30–50 Myr old open clusters IC 2391, IC 2602 and NGC 2547 open clusters. The dotted locus corresponds to a Li abundance $A(\mathrm{Li}) = 3.1$ which approximates a star that has not depleted its initial Li.

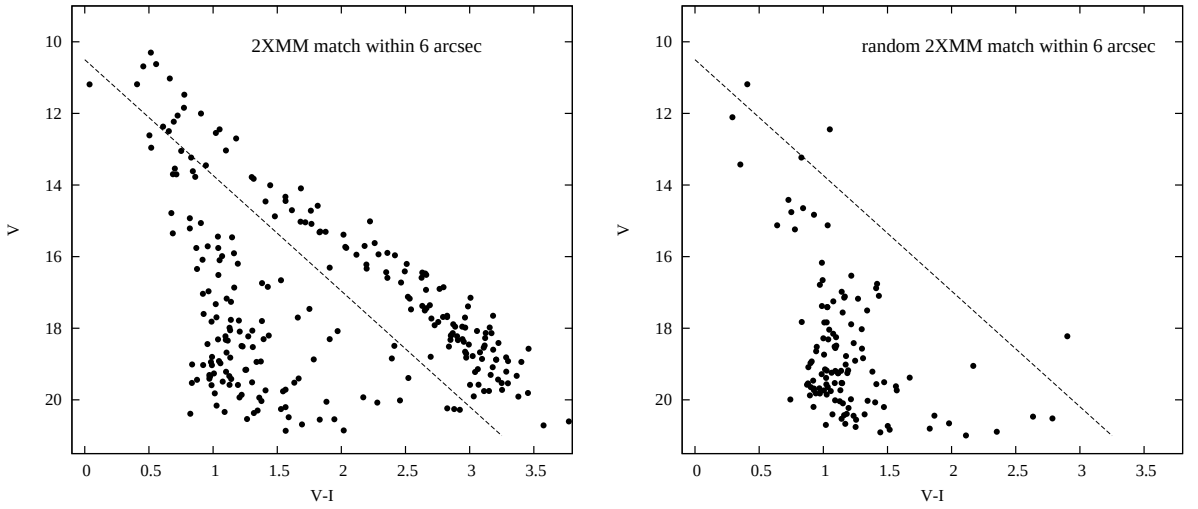

Figure 4. (a) The CMD for unflagged optical sources correlated (up to a maximum of 6 arcsecs) with the merged 2XMM catalogue (see text). (b) The likely distribution of spurious correlation in this CMD, obtained by offsetting all the X-ray sources by 30 arcsecs before performing the correlation. Only 3 correlations above and to the right of the dashed PMS boundary defined in section 2.3 are expected to be spurious.

bars) the empirical upper limit to W[Li] for a 30–50 Myr old star. The usefulness of W[Li] as a youth indicator declines for these warmer stars because the timescale for Li-depletion is longer. However, because all eight have a RV consistent with association membership we assume they are members.

(iv) The five bluest stars in the sample (with $V-I < 0.5$) have only upper limits for W[Li] which might be consistent with undepleted Li. Three are also early-type stars for which we have been unable to ascertain an accurate RV. These three objects could be association members, but equally could be field objects and are classed as "uncertain". The RV of the remaining two objects is incompatible with cluster membership, so we class them as non-members.

(v) The rest of the objects which have only upper limits to their W[Li] are assumed to be non-members of the association. They either have a RV inconsistent with membership or lie far enough below the Li-rich members to make membership unlikely.

A summary of our spectroscopic membership judgements is included as a column in Table 3. All together there are 32 stars considers as members, 49 as non-members and 3 with uncertain membership.

Table 4. (a) X-ray sources from the 2XMM catalogue which are correlated with 131 unflagged PMS optical counterparts in our photometric catalogue (those lying above the locus defined in Fig. 4), appended with the details for 5 sources correlated with PMS counterparts that have flagged photometry, but which were included as spectroscopic targets. Column 1 gives the IAU name of the 2XMM source, column 2 lists which observation the X-ray source parameters come from (1 = the observation beginning on MJD 52013, 2 = the observation beginning on MJD 52033), column 3 gives the source detection likelihood, columns 4–9 gives the count rates and uncertainties in the 0.5-4.5 keV range for the pn, m1 and m2 instruments respectively (a zero here indicates the source was not found in that detector). Column 10 is the separation between X-ray source and optical counterpart,columns 11–12 are the optical counterpart identifiers from Table 2. Columns 13–14 are the RA and Dec (J2000) of the optical source, columns 15 and 16 give the V and $V-I$ of the optical counterpart, column 17 is the average unabsorbed X-ray flux (0.5-4.5 keV, erg cm^{-2} s^{-1}), column 18 the assumed V-band bolometric correction and column 19 the derived X-ray to bolometric flux ratio. (b) A similar table, but for those 124 optical counterparts lying below the PMS selection locus shown in Fig. 4. These tables are only available in electronic form. A sample is shown below to illustrate the content.

(1) IAU Name	(2) Obs	(3) ML	(4) pn (s^{-1})	(5) pn_err (s^{-1})	(6) m1 (s^{-1})	(7) m1_err (s^{-1})	(8) m2 (s^{-1})	(9) m2_err (s^{-1})	(10) Separation (arcsec)
2XMMp J080815.0-471537	2	4.7E+02	0.00E+00	0.0E+00	2.00E−03	2.6E−04	2.50E−03	2.2E−04	0.9
2XMMp J080817.8-472246	2	1.2E+01	1.56E−04	1.8E−04	3.59E−04	9.4E−05	0.00E+00	0.0E+00	1.6
2XMMp J080820.3-472026	2	2.9E+01	9.86E−04	4.8E−04	2.51E−04	7.9E−05	2.69E−04	8.1E−05	2.2
2XMMp J080825.8-471639	1	1.7E+02	2.64E−03	3.7E−04	9.02E−04	1.8E−04	1.06E−03	2.1E−04	1.5
...									

(11)	(12) Identifier	(13) RA	(14) Dec	(15) V	(16) $V-I$	(17) $f_{\rm x}$ (erg cm^{-2} s^{-1})	(18) BC$_V$ (mag)	(19) $\log(L_{\rm x}/L_{\rm bol})$
6	389	122.06241	-47.26055	15.947	2.117	4.10E−14	-1.541	-3.06
3	1670	122.07418	-47.37936	18.599	3.183	3.79E−15	-2.897	-3.57
3	576	122.08422	-47.34054	17.701	2.963	5.39E−15	-2.584	-3.65
12	213	122.10751	-47.27726	16.206	2.509	1.79E−14	-2.000	-3.50
...								

3.2 Membership from the X-ray data

Late-type PMS stars are strong X-ray emitters, with a ratio of X-ray to bolometric luminosity, $L_{\rm x}/L_{\rm bol}$, between 10^{-4} and 10^{-3}. Field stars are not usually such strong X-ray emitters unless they happen to be very young and rapidly rotating or tidally locked in close binary systems. X-ray emission is therefore an excellent way to identify PMS stars, although because the bolometric luminosity of lower mass PMS stars is smaller, an X-ray selected sample will become increasingly incomplete towards fainter objects. The X-ray observations here are deep enough that this limit is approached for much fainter objects than have optical spectroscopy (see below), so an X-ray selected sample has the merit of clean membership selection to lower masses.

The *XMM-Newton* field of view is roughly 30 arcminutes in diameter, so only a subset of the photometric survey is covered by X-ray observations. We looked for correlations between X-ray sources and optical counterparts using a 6 arcsecond correlation radius. We restricted the optical catalogue to those stars with unflagged photometry and uncertainties in V and $V-I$ less than 0.1 mag, finding 255 matches to 202 individual X-ray sources. Randomly offsetting the X-ray positions by 30 arcsecs reveals that about half of these correlations are likely to be spurious because of the large number of optical sources with faint magnitudes. Fig. 4 demonstrates that most spurious correlations will be with faint objects having $V-I \simeq 1$. If we define a line on the CMD running from (0.0,10.5) to (3.25,21), then the obvious PMS locus seen in the cool part of the optical CMD and also the spectroscopic members (see section 3.1) lie above this line, whilst the bulk of the optical catalogue lies below it. Correlating the merged X-ray catalogue against objects lying above the line accounts for 131 of the matches and only 3 of these are expected to be spurious (see Fig. 4 [right]). The conclusion is that the vast majority of X-ray selected PMS candidates (i.e. those above the line) are genuine correlations and that spurious correlations are predominantly fainter and bluer than the cluster members. Tables 4a and 4b list the correlations between the 2XMM and optical catalogues. Appended to Table 4a are details for X-ray sources correlated with five flagged PMS counterparts that were included as spectroscopic targets.

To assess whether the X-ray emission seen is characteristic of young PMS stars we estimate the $L_{\rm x}/L_{\rm bol}$ ratio. We have used the PIMMS (version 3.9e) tool from NASA's High Energy Astrophysics Science Archive Research Center to convert EPIC count rates into unabsorbed X-ray fluxes in the 0.5–4.5 keV energy range. We assume a one temperature Raymond & Smith (1977) thermal corona and that the column density is $\simeq 3\times10^{20}$ cm^{-2}, which is appropriate for a reddening $E(B-V) \simeq 0.04$ (Bohlin, Savage & Drake 1978). We assume an average coronal metallicty of $Z = 0.4$, since it is now well established that active PMS stars exhibit subsolar coronal metallicities of this order (e.g. Scelsi et al. 2007). Finally, we used a mean coronal temperature of $10^{7.0\pm0.1}$ K. This was arrived at by considering the mean hardness ratio and standard deviation (using the 0.5–1 keV and 1–2 keV bands) of 82 PMS objects with good detections in the pn instrument. These assumptions have little effect on the final estimated X-ray fluxes. The count-rate conversion

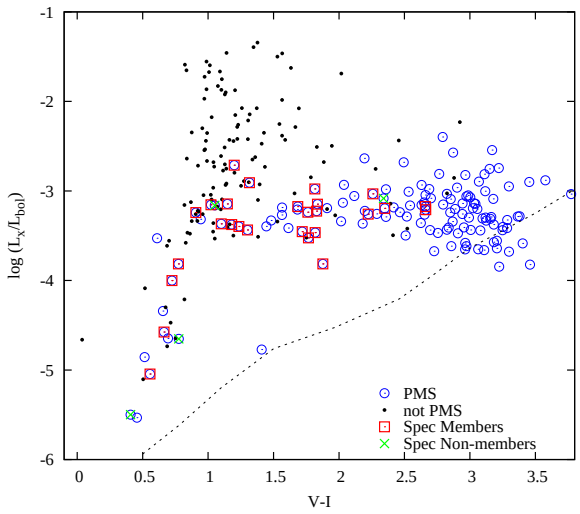

Figure 5. X-ray to bolometric flux ratio, calculated assuming that all the X-ray sources have the coronal spectral parameters discussed in the text and have an extinction/reddening appropriate for the association. Stars which are PMS candidates based upon their photometry (i.e. above the dashed line in Fig. 4) are indicated, as are those which have had their membership confirmed by spectroscopy or otherwise. The dashed line indicates the approximate sensitivity limit of the *XMM-Newton* observations for an object situated in the association PMS.

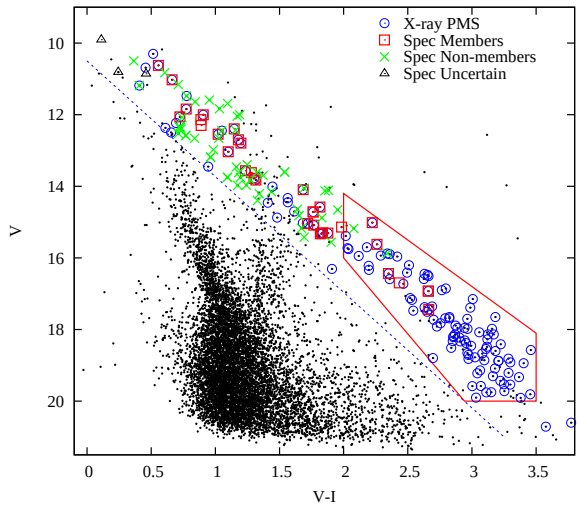

Figure 6. The colour-magnitude diagram for objects from the photometric catalogue within the *XMM-Newton* field of view (small dots). Additional symbols identify X-ray sources with a PMS optical counterpart, along with the membership status of objects we have observed spectroscopically. The polygon defined by the solid line is used to select an almost complete and contamination-free sample of association members (see section 3.3).

factor changes by: $^{+26}_{-10}$% if $\log T$ changes by ± 0.3; decreases by 1% if $Z = 1.0$; and by $^{+11}_{-6}$% if the column density changes by $\pm 3 \times 10^{20}\,\mathrm{cm}^{-2}$.

The final conversion factors we use from pn (or MOS) count rates (in the 0.5–4.5 keV band) to unabsorbed X-ray fluxes (in the 0.5–4.5 keV) band are $2.27 \times 10^{-12}\,\mathrm{erg\,cm}^{-2}$ (or $6.06 \times 10^{-12}\,\mathrm{erg\,cm}^{-2}\,\mathrm{count}^{-1}$), where these conversion factors apply to count rates evaluated over the whole point spread function of the X-ray source (as supplied by the 2XMM catalogue). Bolometric fluxes were calculated using V magnitudes, a bolometric correction derived from the intrinsic $V-I$ (described in Naylor et al. 2002) and assuming $E(V-I) = 0.055$ and $A_V = 0.131$ (see section 4.4). Table 4 lists the average fluxes, assumed bolometric corrections and $\log(L_\mathrm{x}/L_\mathrm{bol})$ for both PMS and non-PMS X-ray sources.

Figure 5 shows the results and clearly demonstrates that the X-ray selected PMS candiates, many of which have been confirmed by our spectroscopy, show activity levels characteristic of PMS populations – a level of activity that increases with $V-I$ as the objects develop deep convection zones, saturating at $L_\mathrm{x}/L_\mathrm{bol} \simeq 10^{-3}$ for cool objects. Note there are four spectroscopic non-members which are indistinguishable from members on the basis of their X-ray activity. It is possible that these are spurious correlations – recall that ~ 3 were expected in the PMS sample, and these are most likely to occur for $V-I < 1.6$ where the density of optical sources contaminating the PMS is greatest (see Fig. 6). There is also one object (ID 12-75) with an X-ray activity level much lower than other PMS candidates with $V-I \sim 1.5$ and is unlikely to be a cluster member. We conclude that an X-ray selected sample of photometric PMS candidates with $V-I > 1.6$ is unlikely to be contaminated. Most of the remaining (non-PMS) X-ray sources will either be active field dwarfs and coronally active binary systems with $L_\mathrm{x}/L_\mathrm{bol} \leqslant 10^{-3}$ or, for the objects with larger X-ray to bolometric flux ratios, active galaxies which are probably not even correlated with the correct optical counterpart.

The minimum detectable unabsorbed X-ray flux in the *XMM-Newton* observations is roughly $1.5 \times 10^{-15}\,\mathrm{erg\,cm}^2\,\mathrm{s}^{-1}$ when calculated using the conversion factors discussed above. The dashed line in Fig. 5 shows how this translates into a $L_\mathrm{x}/L_\mathrm{bol}$ detection threshold for a typical object that is part of the X-ray selected PMS. As the X-ray luminosity functions of PMS stars are not bimodal and there is a significant gap between the $L_\mathrm{x}/L_\mathrm{bol}$ threshold and the detected PMS stars. There are 5 spectroscopically confirmed members which are apparently not X-ray sources in Fig. 6. In fact 3 of these are outside the *XMM-Newton* field of view (ID 16-40, ID 6-216 and ID 8-24). One of them (ID 4-41) lies in the wings of a bright X-ray source and is probably confused within it, and the final object (ID 10-97) lies just over 6 arcsecs from an X-ray source correlated with another spectroscopic member (ID 10-93). It is likely that two separate X-ray sources have been merged by the *XMM-Newton* spatial resolution and subsequent analysis. We can conclude that X-ray selection will be almost complete (where there is X-ray coverage) for PMS stars with $V-I < 2.8$, $V \simeq 18$, but increasingly limited to the most active of stars that are even cooler.

3.3 Photometric membership

Whilst an X-ray selected sample can be defined which is complete and uncontaminated for $1.6 < V-I < 2.8$, this sample is spatially limited to the 650 arcmin^2 *XMM-Newton* field of view. The photometric survey is more extensive so it makes sense to also define a photometrically selected sample. Fig. 6 shows the CMD within the X-ray field of view and

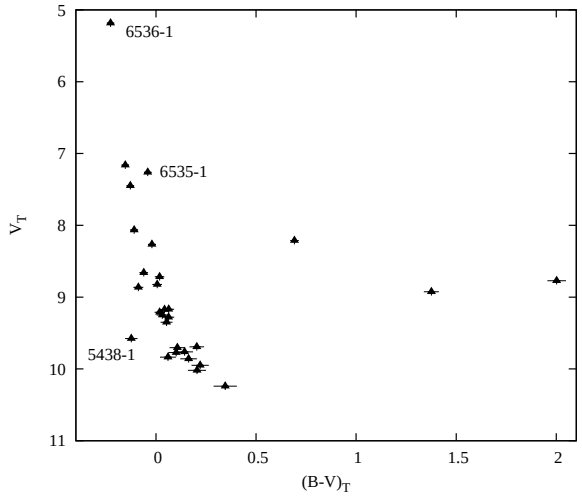

Figure 7. The colour-magnitude diagram for objects in the Tycho Catalogue within 45 arcminutes of γ Vel and which satisfy a proper motion criterium (see text).

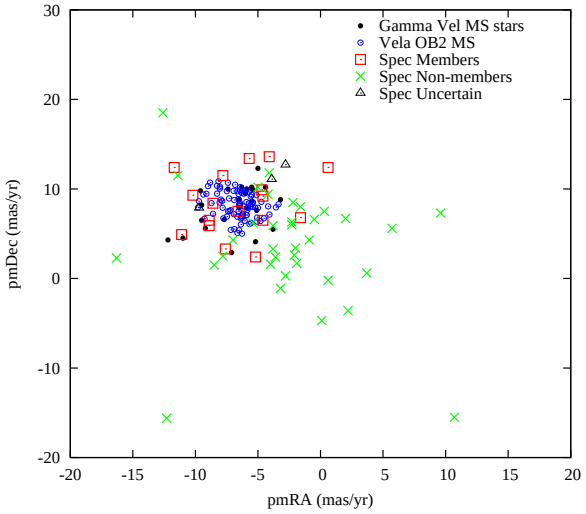

Figure 8. Proper motions for the various stellar samples discussed in the text. The γ Vel and Vela OB2 main-sequence proper motions come from the Tycho and Hipparcos catalogues respectively. The proper motions for the spectroscopic targets are good quality measurements from the NOMAD catalogue.

demonstrates that, for $2 < V - I < 3$, the vast majority of photometric PMS candidates (those above the dashed line) are X-ray sources with $L_{\rm x}/L_{\rm bol} > 10^{-4}$ and therefore likely to be very young stars. For hotter PMS candidates there are an increasing proportion which are not X-ray sources or are proven spectroscopic non-members. For cooler candidates a lack of X-ray sensitivity probably leads to an increasing fraction of non-detections. Note that Fig. 6 plots data for all of our spectroscopic targets, some of which lie outside the *XMM-Newton* field of view. In particular, there are eight spectroscopic members in Fig. 6 that appear not to be X-ray sources. In fact, three of these lie outside the *XMM-Newton* field (ID 6-216, ID 8-24 and ID 16-40), while the remaining five have flagged photometry.

For the purposes of judging the spatial distribution of cluster members we define a selection box as shown in Fig. 6 which should result in a sample of PMS candidates with $V - I > 2$ that are nearly uncontaminated and complete for $V \leqslant 20$, the approximate completeness limit of the photometric survey. To put this on a quantitative basis, there are 24/116 objects in this photometric selection box that are *not* X-ray sources or are spectroscopic non-members. However, the majority of these have $V > 18$ and have probably just not been detected in X-rays *yet*. This means that the contamination level is $< 0.037\,{\rm arcmin}^{-2}$ if we assume all the X-ray sources in the selection box are members of the association. Applying the selection box to the full photometric catalogue defines a sample of 319 unflagged photometric members with $V < 20$.

3.4 Membership of bright stars

The saturation level of our new CCD photometry is $V \simeq 10.5$. To get information on brighter stars we consult the Tycho-2 catalogue (Høg et al. 2000) which contains V and $B - V$ magnitudes in the Tycho system along with precise positions and proper motions.

To define a sample of bright association candidates we take those stars within 45 arcminutes of γ^2 Vel that satisfy two further criteria. (i) Their proper motions are within three times their error bar of the mean proper motion of the Vela OB2 association derived from Hipparcos data by de Zeeuw et al. (1999). We add 1 mas/year in quadrature to the proper motion uncertainty (corresponding to $\simeq 1.5\,{\rm km\,s^{-1}}$ in tangential motion) to account for any small velocity dispersion (see section 4.1). (ii) They have photometric uncertainties of < 0.05 mag in V and $B - V$ (in the Tycho system). This proper motion and position selection results in the catalogue of 29 stars shown in Fig. 7. There are three objects with $B - V > 0.5$ (Tyc-8140-4503-1, Tyc-8140-2697-1, Tyc-8140-3771-1) which clearly stand out as anomalous. These are most likely unrelated background giants – they would have to be $> 300\,{\rm Myr}$ old if they were red giants at the distance of the association.

The majority of the stars selected form a sequence in colour-magnitude space (Fig. 7), and share the same proper motion. It is quite likely they are a distinct, co-eval population. Since they share the same position on the sky as our PMS sample, it is also likely that both groups are part of the same population. Indeed, it is almost inconceivable that the two are not the same population, since were they not, the question would be where in the CMD are the higher-mass stars which correspond to the large number of low-mass stars we have found (see section 4.7)?

4 PROPERTIES OF THE ASSOCIATION AROUND GAMMA VEL

4.1 Kinematic and spatial coherence

Figure 3 shows that the Li-rich stars are closely grouped in RV. If we take the 27 spectroscopically confirmed PMS candidates that have $11 \leqslant RV \leqslant 22\,{\rm km\,s^{-1}}$, then the mean association heliocentric RV is $17.1\,{\rm km\,s^{-1}}$ with a standard deviation of $2.5\,{\rm km\,s^{-1}}$. This standard deviation must be a strong upper limit to the 1-dimensional velocity dispersion

in the cluster. We estimate that the RVs are uncertain at the level of 2–3 km s^{-1}, which must account for the majority of the observed dispersion. No external RV standards (other than the Sun) were observed during our spectroscopy run. Experience from other datasets suggests that the uncertainty in the mean RV will be dominated by systematic effects at the level of $\sim \pm 1$ km s^{-1}, rather than the smaller statistical uncertainty in the mean.

The systemic RVs of γ^1 and γ^2 Vel are 9.7 ± 1.0 and 7 ± 23 km s^{-1} respectively (Hernandez & Sahade 1980; Schmutz et al. 1997). The very small error bar on the RV of γ^1 Vel should be treated with caution. These were photographic spectra with RVs averaged over many spectral lines. It is unclear how the line centres were determined or whether there was significant variation between lines. No systematic study of the RVs of other early-type stars near γ Vel has been reported.

Proper motions for the Vela OB2 main sequence (MS) stars and the bright Tycho-selected MS stars around γ Vel are available from the Hipparcos and Tycho catalogues respectively, and have typical uncertainties of 0.8 and 1.5 milliarcsec/year in each coordinate. We searched the NOMAD catalogue (Zacharias 2005) for proper motions for fainter sources in our optical catalogue. Good quality proper motions (flagged as of astrometric standard) are available for 58 of the 84 stars with spectroscopic membership determination. All of these have $V < 15.5$ and uncertainties of ~ 5 milli-arcsec/year in each coordinate.

The proper motions are plotted in Fig. 8 and the mean and standard deviations of the proper motion for each of these stellar groups are reported in Table 5. Note that the MS stars around γ Vel and the Vela OB2 stars have been selected on the basis of their similar proper motions, yet may still contain some non-members. The key point is that the spectroscopic members are indistinguishable from γ^2 Vel, the Vela OB2 MS stars and the MS stars around γ Vel on the basis of their proper-motions. The mean proper motions agree to within their small statistical uncertainties and the observed standard deviations are close to the statistical uncertainties, suggesting that any internal scatter in the proper-motions is small. Quantitatively, the internal scatter is probably less than 1.5 milli-arcsec/year for the MS stars around γ Vel (< 2.5 km s^{-1} at the distance of γ Vel, see section 4.2) and consistent with zero for the spectroscopic members. On the other hand the spectroscopic non-members show a larger dispersion and a different mean proper-motion. On that basis it seems likely, although not conclusive, that the 3 stars with "uncertain" status (triangles in Fig. 8) are members. Given sufficiently precise proper motions (of order 2 milliarcsec/year) it should be possible to separate cluster and field populations with some confidence. However the proper motions we have are limited to relatively bright stars ($V < 16$) and are quite incomplete, so cannot be effectively used for that purpose in this paper.

To examine the spatial structure of the low-mass association we use the photometrically defined sample of PMS candidates (section 3.3). This covers the entire photometric survey and should have reasonably uniform spatial sensitivity apart from the region immediately around γ^2 Vel itself (see section 2.1).

Figure 9a shows the spatial distribution of the 319 photometric candidates from the selection box in Fig. 6. The

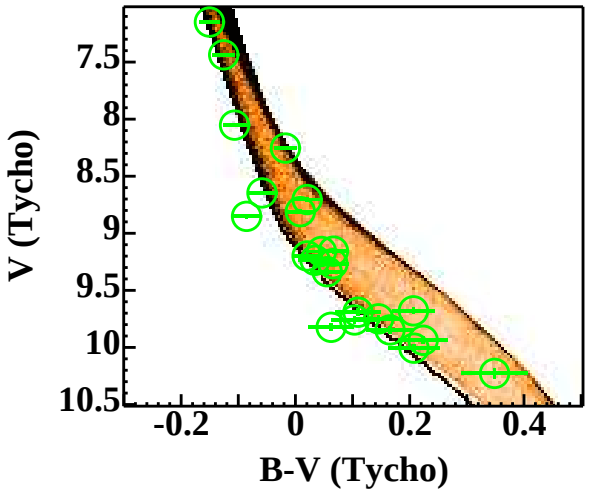

Figure 10. The best fitting model (colour scale) to the dataset of Figure 7.

radial distribution of these objects is shown in Fig. 9b, centred on γ^2 Vel. We have made a correction (which is only significant for the first two bins) for spatial incompleteness in the survey, by normalising to the radial distribution of stars selected from a comparison box in the $V, V-I$ CMD with $V-I < 2$ and $16 < V < 20$. An upper limit to the level of contamination (derived from < 24 non-members in the 650 arcmin^2 *XMM-Newton* field of view) is also shown.

A clear central concentration in the spatial distribution of photometric association candidates is evident. But it is also apparent that the edge of the spatial distribution has not been reached, because the spatial density of candidates members is still significantly higher than the upper limit to the background level even at radii of 0.5–0.6 degrees.

4.2 Distance and Extinction for a main sequence sample

The low-mass stars identified as young association members based on their RVs, lithium abundance and X-ray emission, are PMS stars which fade as they contract. The sequence they form moves to fainter magnitudes with age, resulting in a strong age-distance degeneracy if we were to try and fit that sequence with model isochrones (e.g. Naylor & Jeffries 2006). Conversely, high-mass stars around γ Vel have already reached the MS, with almost age-independent positions in a CMD (for a quantitative discussion see Mayne & Naylor 2008). By measuring the distance to these we can pin down the distance to the low-mass objects and hence get a better age estimate.

Later we shall show that the MS sample around γ Vel is at a similar distance to the majority of the Vela OB2 association, and that γ Vel itself also lies at this distance, but for the moment one should be quite clear that fitting the proper-motion-selected MS sample from section 3.4 does not actually measure the distance to either γ Vel or Vela OB2.

We fitted the MS dataset from section 3.4 using the Geneva-Bessell models described in Mayne & Naylor (2008). These are based on the Geneva isochrones (Lejeune &

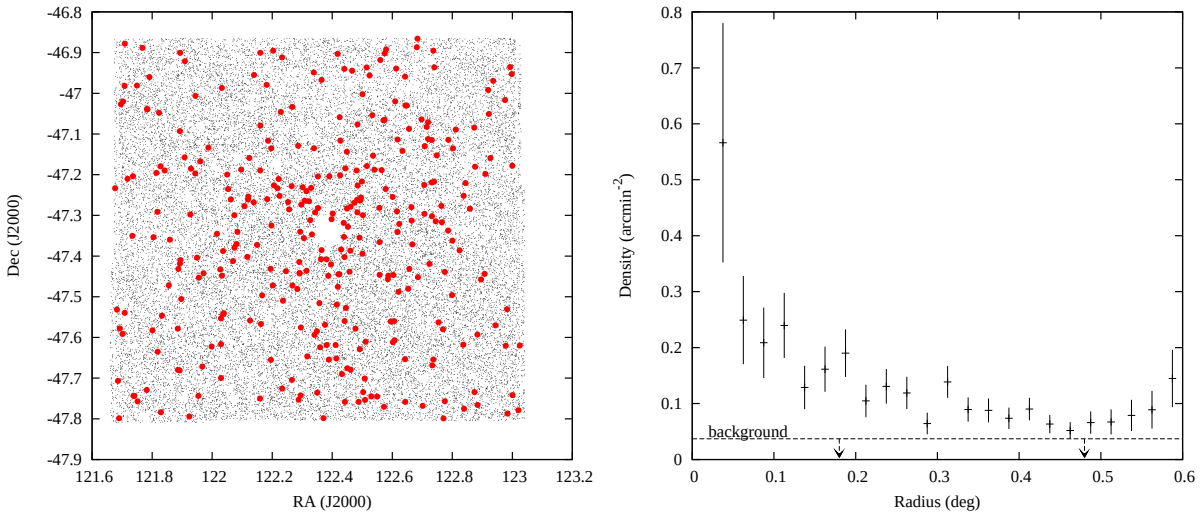

Figure 9. (a) Large spots show the locations of the low-mass PMS photometric candidates defined in section 3.3. The small dots show the quasi-uniform distribution of the much larger number of stars with similar brightness (but bluer colours). The "hole" in the middle is caused by the lack of good photometry for stars that are close to γ^2 Vel. (b) The radial distribution of the photometric PMS candidates, normalised by the radial distribution (centred on γ^2 Vel) of the comparison sample with similar brightness. The central bin is missing because no good photometry was obtained close to γ^2 Vel. The horizontal dashed line shows an upper limit to the level of contamination in the sample.

Group	Nstars	Avg. uncertainty (mas/yr)	pm RA (mas/yr) mean	pm RA (mas/yr) std. dev.	pm Dec (mas/yr) mean	pm Dec (mas/yr) std. dev.
γ^2 Vel	1	–	−5.9	0.5	+9.9	0.4
Vela OB2 MS	85	0.8	−6.6	1.3	+8.1	1.4
γ Vel MS	24	1.5	−6.8	2.2	+7.9	2.4
Spectroscopic Members	17	4.4	−6.5	3.2	+8.5	3.3
Spectroscopic Non-Members	38	4.1	−3.2	6.8	+4.1	11.5

Table 5. A summary of the the proper-motion properties of various star samples (see text).

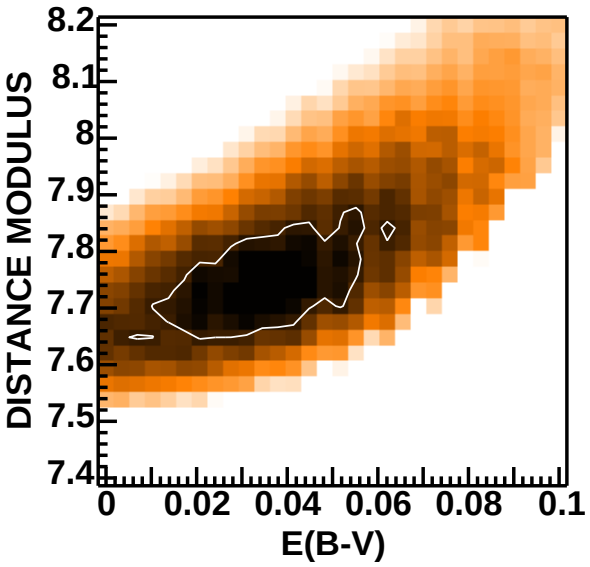

Figure 11. τ^2 as a function of distance modulus and extinction for the data and model of Figure 10. The contour shows the 68 percent confidence region.

Schaerer 2001) but use bolometric corrections and $T_{\rm eff}$-colour conversions from Bessell et al. (1998), assuming the magnitude of Vega is zero in both V and B. These are converted from the conventional BV system to the Tycho system using formulae in Bessell (2000). Using these models to simulate roughly a million stars allowed us to create a probability density for the position of a star in the CMD plane (the colour scale in Figure 10). We then used the τ^2 statistic (Naylor & Jeffries 2006; Naylor in prep.) to compare the model and data for any value of distance modulus and extinction, and find best-fitting values.

Before commencing we removed the three objects with $B-V > 0.5$ (see section 3.4). In addition we removed the star (Tyc-8140-5438-1) which lies too blue of the MS (see Fig. 7). Finally, our bolometric correction runs out at $V_0 \approx -1.7$, which for reasonable distances places star Tyc-8140-6536-1 quite close to the brightest available model. We therefore removed this point as well. We fitted the resulting dataset to a 7 Myr isochrone using the colour-dependent extinction vectors derived for the Tycho system in Mayne & Naylor (2008) and assuming a binary fraction of 50 per cent. Mayne & Naylor (2008) show that the best-fit extinction and distance are not very dependent on the assumed isochronal age, because the fitted stars are much fainter than the MS turn-off. If we fit the resulting dataset without any clipping

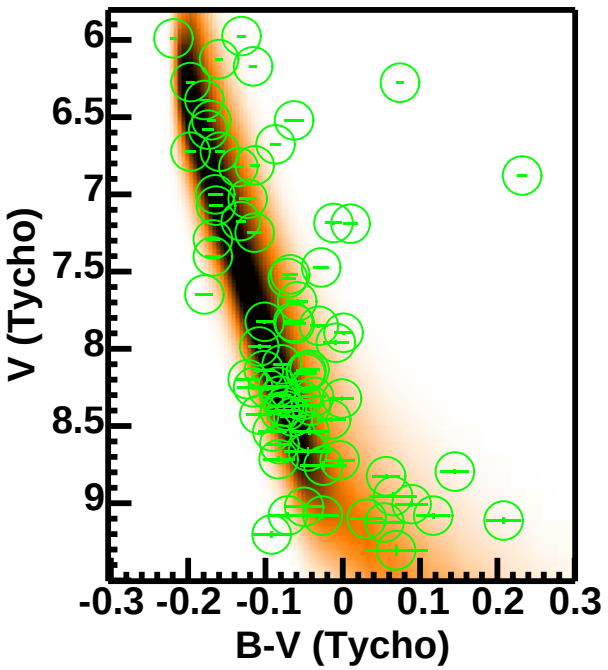

Figure 12. The best fitting model (colour scale) to the 77 Vela OB2 association members defined by de Zeeuw et al. (1999) and which have $V_T > 6$ and $(B-V)_T < 0.5$. The model includes a distance modulus spread of 0.3 mag.

of high τ^2 datapoints (see Naylor & Jeffries 2006) we obtain a $P_r(\tau^2)$ of 0.15 with a distribution of τ^2 which suggests that star Tyc-8140-6535-1, a bright star just to the red of the sequence should also be removed from the fit. Removing this point results in a $P_r(\tau^2)$ of 0.64, and the fit shown in Figure 10. We considered the possibility that both Tyc-8140-6535-1 and Tyc-8140-5438-1 should be included because they represent a real spread in distance. However, these stars lie over a magnitude (in opposite directions) from the sequence, making such an interpretation unlikely.

The plot of τ^2 as a function of distance and extinction (analogous to a χ^2 space), is shown in Figure 11. Since we have a reasonable $P_r(\tau^2)$ value we calculate parameter uncertainties as described in Naylor (2008 in prep),without any need to increase the uncertainties for the individual datapoints. Doing so results in the confidence interval shown in Fig. 11. The lowest τ^2 (corresponding to the most likely parameter values) occurs at an absolute distance modulus of 7.76 ± 0.07 mag and $E(B-V)$ of 0.038 ± 0.016 mag, where the uncertainties are 68 per cent confidence levels for one parameter of interest.

4.3 The Distance to Vela OB2

To establish a distance to the surrounding Vela OB2 association on the same basis we fitted Tycho photometry of the members given by de Zeeuw et al. (1999). These stars were chosen by de Zeeuw et al. on the basis of photometry and proper motions and lie in a region more than 10 degrees in diameter. We again limited ourselves to stars with $V_T > 6$, due to the limitation of our calibration, and ignored objects

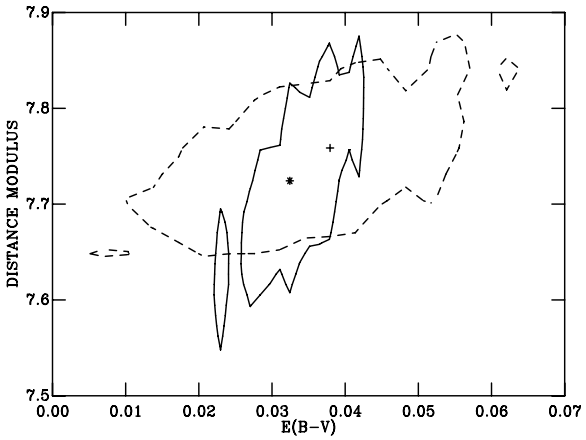

Figure 13. The 68 percent confidence limits in intrinsic distance modulus and extinction for the de Zeeuw sample (solid contour) and the MS sample around γ Vel (dashed contour). The asterisk and cross respectively mark the best-fit values for these samples.

with $(B-V)_T > 0.5$, since these are either non-members, or perhaps evolved stars.

Such a fit, using a clipping threshold of τ^2=10, clips 19 of the 77 available datapoints, and still only achieves $P_r(\tau^2) = 0.00004$. The absence of a clearly defined sequence implies that there may be a spread in distance. We modelled this as a spread in distance modulus, by convolving a Gaussian with the expected distribution in colour-magnitude space. This procedure cannot be carried out in a statistically rigorous fashion, since adding the distance modulus spread changes the number of datapoints which are clipped out. This ruins any chance of a strict statistical comparison between models with different distance spreads, but in any case clipping is not a well defined process in statistical terms. However, if we introduce a Gaussian spread in distance modulus with $\sigma = 0.3$ mags, then $P_r(\tau^2)$ rises to about 0.52 for only 13 clipped datapoints. Furthermore the distribution of τ^2 for the unclipped points is similar to that predicted from the model. Introducing the distance spread has little effect on the derived best-fit parameters, changing the distance modulus and $E(B-V)$ from 7.65 and 0.028 mag respectively to 7.68 and 0.036 mag.

To derive a reasonable estimate of the uncertainties for the model with a distance spread we repeat the τ^2 grid search with the clipped datapoints removed. We find a best-fitting $E(B-V) = 0.032 \pm 0.009$ mag and absolute distance modulus of 7.72 ± 0.08 mag. The best-fitting model (with a distance modulus spread of 0.3 mags) is shown with the data overlayed in Figure 12. The 68 percent confidence contour is plotted on Fig. 13. It is clear that the sample of MS stars around γ Vel and the de Zeeuw Vela OB2 sample have an indistinguishable distance modulus and extinction at this level.

The distance modulus we have found for the Vela OB2 sample is closer than the (8.06±0.07) mag found by de Zeeuw et al. (1999). We have no definitive explanation for this. There have been problems with reported mean Hipparcos parallaxes to some clusters and associations (notably the Pleiades – see Pinsonneault et al. 1998) probably due to correlated parallax errors over small regions on the sky. Another factor may be the accuracy of the correction de Zeeuw

et al. have applied to account for biases introduced by discarding objects with negative parallax and incompleteness for stars with fainter magnitudes. A further possibility is a departure from our assumption of solar metallicity. This is discussed further in section 5.

The suggestion of a ± 0.3 mag spread in distance modulus is not altogether surprising. The stars defined as the Vela OB2 association by de Zeeuw et al. (1999) occupy a roughly circular area of about 12 degrees diameter. If the association is spherical then the front-to-back distance spread would be of order ± 0.2 mag. There also remains the possibility of small star-to-star reddening variations which if modelled as a vertical displacement in the CMD could mimic a significant distance spread.

4.4 The Age of the Pre-Main-Sequence Sample

4.4.1 Low-mass PMS model isochrones

To determine an age for the PMS sample we adopt the best fitting distance modulus and extinction from fitting the MS stars whose projected positions lie around γ Vel (see section 4.2). Extinction and reddening in terms of A_V and $E(V-I)$ are calculated for a star with a typical intrinsic PMS colour as $A_V = 3.48E(B-V) = 0.131$ and $E(V-I) = 1.44E(B-V) = 0.055$ (see Bessell et al. 1998).

A model dependent absolute age can be estimated by comparing the PMS data to model isochrones. In practice this is difficult to do. Figure 14 shows various attempts to match a PMS sample around Gamma Vel, consisting of the spectroscopic and X-ray selected photometric members defined in section 3, using different models. The top left panel shows Siess et al (2000) isochrones overlaid on the data. These are the $Z = 0.02$ models, with a relationship between colour and effective temperature that is tuned to match photometry in the Pleiades, as described in Naylor et al (2002). If we restrict ourselves to $V-I < 2.5$ where we know our photometric calibration is excellent, then the lower envelope of the data suggests ages of 10–12 Myr, whilst the upper envelope suggests ages < 5 Myr. Of course our data doubtless contain many binaries which are up to 0.75 mag brighter than a single star of the same colour, but even so, the redder stars have a magnitude spread which is larger than this, perhaps indicating a real age spread. For $V-I > 2.5$ the data dip well below the 10 Myr isochrone in a way not reproduced by the Siess et al isochrones, either due to inadequacies in the cool model atmospheres or possibly in the photometric calibrations for very red stars.

The top right panel of Fig. 14 shows a similar comparison using the mixing length 1.0 isochrones from Baraffe et al. (2002), again with the bolometric corrections and colour-effective-temperature relations outlined in Naylor et al (2002). The bottom left panel shows the same comparison with the models of D'Antona & Mazzitelli (1997). The data for $V-I < 2.5$ in these diagrams suggest that the oldest single stars have ages of 15–20 Myr and 7–10 Myr respectively, with the same discrepancies for cooler stars. The distance uncertainty for the γ Vel association makes little difference to these numbers and the reddening vector runs almost parallel to the isochrones.

A further factor to be considered is the choice of colour-temperature conversion relation. In the bottom right panel of Fig. 14 we show the results of transforming the Siess isochrones using the often-used colour-temperature relationship of Kenyon & Hartmann (1995). Obviously the data are far from parallel to these isochrones. The age of the association would be 5–15 Myr, depending on which colour range was considered. Finally, all these models are roughly at a solar metallicity. Relaxation of this assumption is discussed in section 5.

4.4.2 Low-mass PMS empirical isochrones

An alternative approach is to consider empirical isochrones. In Fig. 15a we compare our data to empirical isochrones for the σ Ori, λ Ori, NGC 2362 and 25 Ori clusters. These isochrones were constructed by fitting low-order polynomials or splines through published datasets of low-mass members (see Mayne et al. 2007; Mayne & Naylor 2008) and adjusting the distance moduli and reddening to match those assumed for the γ Vel association. For σ Ori, λ Ori and NGC 2362 we used distances and reddening consistently rederived for early-type members (using the same techniques as described here) by Mayne & Naylor (2008), whereas for 25 Ori we used the intrinsic distance modulus of 7.59 and $A_V = 0.29$ derived by Briceño et al. (2007).

Figure 15a suggests that the PMS stars around γ Vel are older than those of the σ and λ Ori clusters, which have been assigned ages of $\simeq 3$ Myr in the empirical age ladder of Mayne & Naylor (2008), older than NGC 2362 which is assigned an age of 4–5 Myr and similar in empirical age to the PMS stars of the 25 Ori cluster, which Briceño et al. (2007) concluded had an age of 7–10 Myr, based mainly on Siess isochrones. A similar empirical analysis for the γ Vel association using $V-J$ colours was performed by Hernández et al. (2008, see their Fig. 9), assuming an intrinsic distance modulus of 7.72 and $A_V = 0.15$. They also concluded that the γ Vel PMS stars were older than those in σ and λ Ori, but found they were younger than those in 25 Ori.

4.4.3 Lithium depletion

Lithium is strongly depleted in cool stars as they age. The W[Li] values for the γ^2 Vel PMS candidates are shown in Fig. 3b, along with a locus marking the level of undepleted Li. There is no strong evidence for Li depletion in any of the candidates with the appropriate RV (see section 3.1). Theoretically, as a cluster ages we expect to see Li depletion beginning in PMS stars with effective temperatures of 3600–3800 K at ages of 10–20 Myr (Baraffe et al. 1998; Siess et al. 2000, see also Fig. 9 of Jeffries et al. 2003). At older ages a "Li-depletion chasm" opens up towards both higher and lower temperatures. A $T_{\rm eff}$ of 3600–3800 K corresponds to an observed $V-I$ of 2.65–2.25 in this association, so we have observed a few stars which might be expected to show Li-depletion if they were older than 10 Myr. That stars with $V-I > 2.25$ show little or no Li-depletion allows us to put an upper limit to their age of 20 Myr using the Baraffe et al. (1998) models (with mixing length parameter of 1.0 or 1.9 pressure scale heights) or 10 Myr for the $Z = 0.02$ Siess et al. (2000) models. The D'Antona & Mazzitelli (1997) models predict that all stars within $3600 < T_{\rm eff} < 4500$ K ($2.6 > V-I > 1.3$) would be Li-depleted even at 5 Myr, which is clearly incompatible with the data.

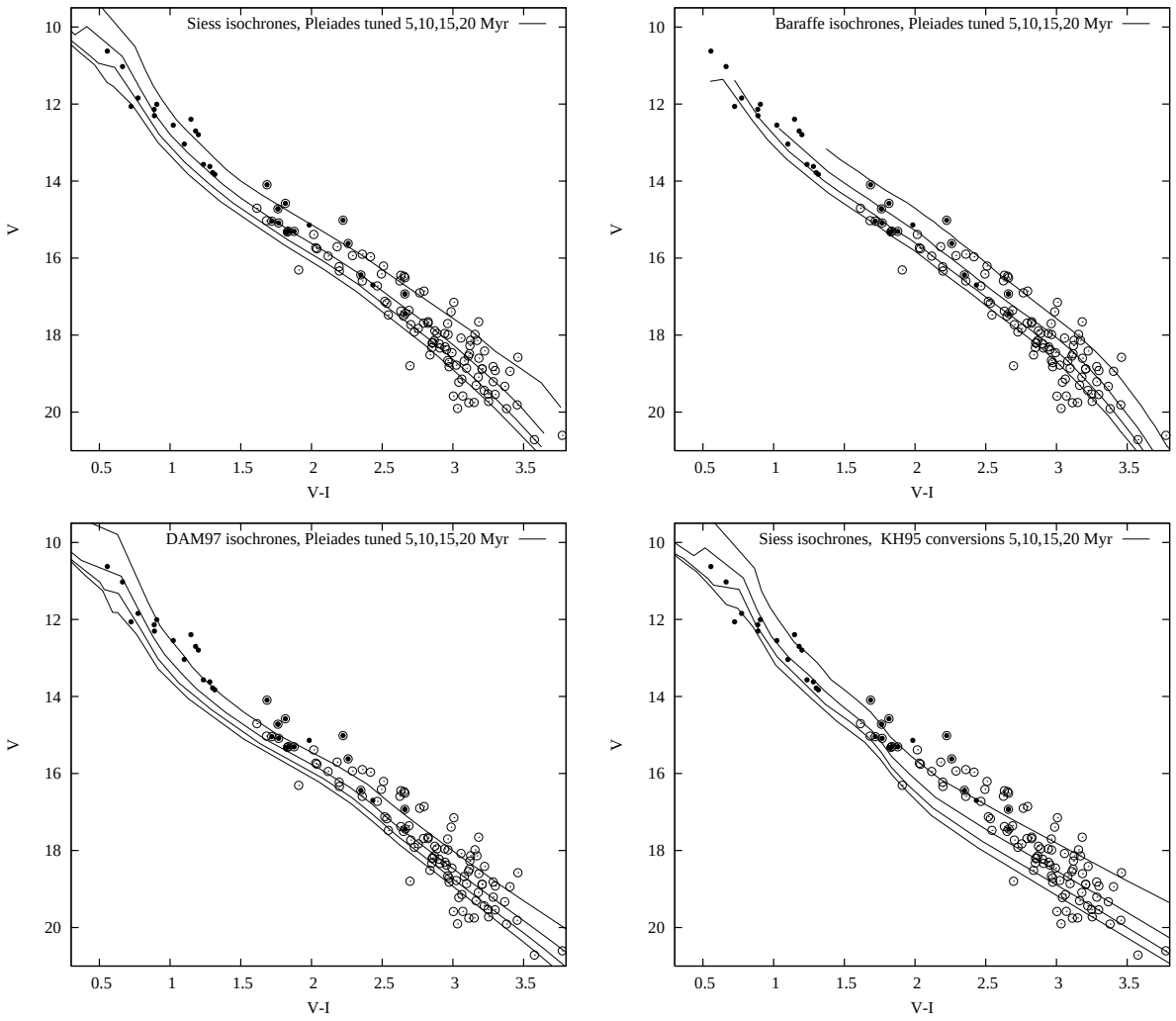

Figure 14. (a) A comparison of low-mass γ Vel PMS association members with evolutionary isochrones in the V vs $V-I$ CMD. The isochrones have been shifted to an intrinsic distance modulus of 7.76 mag, an extinction $A_V = 0.131$ and reddening $E(V-I) = 0.055$. The isochrones are calculated from the $Z = 0.02$ Siess et al. (2000) models, using a colour-temperature relationship tuned to match the Pleiades (see Naylor et al. 2002). Dots show spectroscopically confirmed members, open circles are X-ray selected members. (b) A similar comparison using the Baraffe et al. (2002) models with a mixing length of 1.0 pressure scale heights. (c) A similar comparison using the D'Antona & Mazzitelli (1997) models. (d) A similar comparison to (a) but using the colour-temperature conversions from Kenyon & Hartmann (1995).

We can also consider Li-depletion empirically. The comparison clusters in Fig. 15a also have W[Li] measurements, some of which we show in Fig 15b, a plot of W[Li] versus intrinsic colour. For NGC 2362 we take values for photometry and W[Li] from Dahm (2005). $E(V-I)$ was taken to be 0.04 mag following Mayne & Naylor (2008). For 25 Ori the photometry and W[Li] come from Briceño et al. (2007) and we use their $E(V-I)$ of 0.12 mag. Differences in the definition of continuum levels and spectral resolution in the various analyses may lead to systematic offsets in the W[Li] values, but it is clear that the PMS stars around γ Vel are more akin to those of NGC 2362 in terms of Li depletion. In 25 Ori there seems to be a population of Li-depleted stars that are not present in the γ Vel sample. If it is assumed that 25 Ori has an age of 7–10 Myr then the PMS around γ Vel appears to have an age less than this. A caveat is that the 25 Ori data have much lower resolution ($\simeq$ 6Å) than the spectra analysed here.

4.4.4 Summary of PMS age estimates

In summary, from isochrones in the CMD, PMS stars around γ Vel are at ages of 5–10 Myr on the age scale commonly adopted for other young star forming regions and clusters. There may be a small spread in ages around a single value. This empirical age agrees most closely with the age obtained by comparison with the D'Antona & Mazzitelli (1997) and Siess et al. (2000) isochrones, but is much younger than the age indicated by the Baraffe et al. (2002) isochrones. The evidence from the (absence of) lithium depletion also gives an age < 10 Myr according to the Siess et al. (2000) models and an empirical age of < 10 Myr by comparison with other

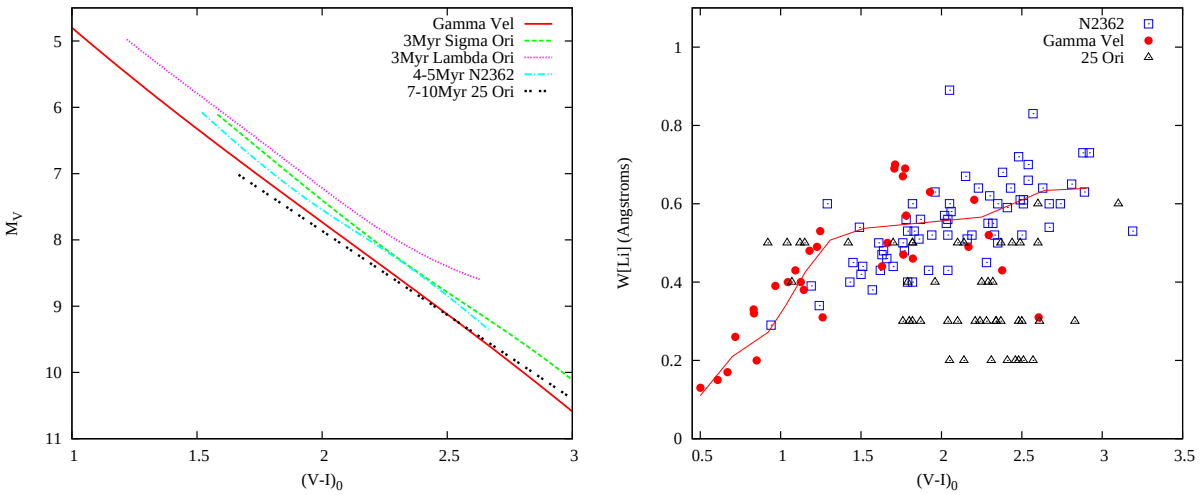

Figure 15. (a) A comparison of the γ Vel PMS association empirical isochrone with empirically determined isochrones for other clusters/associations in the absolute V vs intrinsic $V-I$ CMD. These isochrones have been shifted according to their individual intrinsic distance modulus, extinction and reddening (see text). The red solid line is a third order polynomial fit to the γ Vel PMS data compared to similar representations for the σ and λ Ori clusters (age 3 Myr, Mayne & Naylor 2008), NGC 2362 (age 4–5 Myr, Mayne & Naylor 2008) and the 25 Ori cluster (age 7–10 Myr, Briceño et al. 2007). (b) An empirical comparison based on the EW of the Li 6708Å feature versus intrinsic $V-I$ colour. Data are shown for NGC 2362, the 25 Ori cluster and the PMS around γ Vel. The W[Li] values for 25 Ori are quantised in 0.1Å steps. The solid line shows the locus of undepleted Li defined in section 3.1.

clusters. For the rest of the paper we adopt an age of 7 Myr, but ages of 5–10 Myr are possible.

4.5 The age and mass of γ Vel

North et al. (2007) use their interferometric distance to estimate an absolute V magnitude of -5.63 ± 0.10 for the O-star component of γ^2 Vel, and that it has a mass and age of $28.5 \pm 1.1\,M_{\odot}$ and 3.5 ± 0.4 Myr using the solar-metallicity evolutionary models of Meynet et al. (1994). This is significantly younger than our estimates for the low-mass PMS population. Even incorporating rapid rotation into the model (e.g. Meynet & Maeder 2003) would not increase this age by more than 20 per cent.

The initial mass and lifetime of the WC8 component are more uncertain. North et al. (2007) find an absolute magnitude of -4.23 ± 0.17 and a present day mass of $9.0 \pm 0.6\,M_{\odot}$. If we assume that the eccentric orbit of γ^2 Vel makes it unlikely that there has been Roche-lobe overflow during its lifetime, then the WC8 progenitor probably did not become a red supergiant, which leads to a lower limit to its initial mass of $M > 40\,M_{\odot}$ according to the models of Meynet & Maeder (2003). The same models suggest that the age of a (non-rotating) $M > 40\,M_{\odot}$ WC8 star is < 5 Myr. Agreement with the O-star age of 3.5 Myr would require the initial mass of the WC8 component to be 60–80 $M_{\odot}$.

γ^1 Vel does not feature in the Hipparcos or Tycho catalogues, but has $V = 4.27$, $B-V = -0.23$ (from the preliminary 5th revised edition of the bright star catalogue by D. Hoffleit and W. H. Warren [1991] held by the NASA Astronomical Data Center), a spectral type of B2III and is an SB1 system (Hernández & Sahade 1980). For the distance modulus and extinction derived for the MS around γ Vel this gives an absolute magnitude of -3.62 and an intrinsic $B-V$ of -0.27. If we assume uncertainties of ± 0.02 on the photometry and compare with the solar metallicity evolutionary models of Lejeune & Schaerer (2001), the age could be anywhere between 3 and 15 Myr, with a best fit at an age of 8 Myr and a mass of $14\,M_{\odot}$.

4.6 Circumstellar Material

Young PMS stars often show Hα emission, either as a consequence of rapid rotation and magnetically generated chromospheric activity or due to continued accretion from a circumstellar disk. The Hα emission line in accreting stars (often called classical T-Tauri stars - CTTS) is systematically stronger and broader than in weak lined T-Tauri stars (WTTS), where the emission appears to be mainly chromospheric.

In Fig. 16a we show the EW of the Hα lines of the spectroscopically confirmed γ Vel members as function of colour. Also shown is an empirical dividing line between CTTS and WTTS. White & Basri (2003) defined this dividing line in terms of spectral type and it has been converted to observed $V-I$ colour using the conversion table of Kenyon & Hartmann (1995).

Hernández et al. (2008) analysed Spitzer infrared observations of the γ Vel association members. On the basis of near- and mid-infrared colours they were able to classify stars as discless (class III), having optically thick inner dust discs (class II), discs in transition between class II and class III (transitional or pre-transitional discs) or stars showing only a mid-IR excess (debris discs). In our sample of 32 spectroscopic members there are three examples of stars with debris discs and one with a pre-transitional disc. The rest are classed as discless class III objects. The stars with discs are indicated in Fig. 16a.

From Fig. 16a we see that only the star classified as a pre-transitional disc object has an Hα EW large enough to

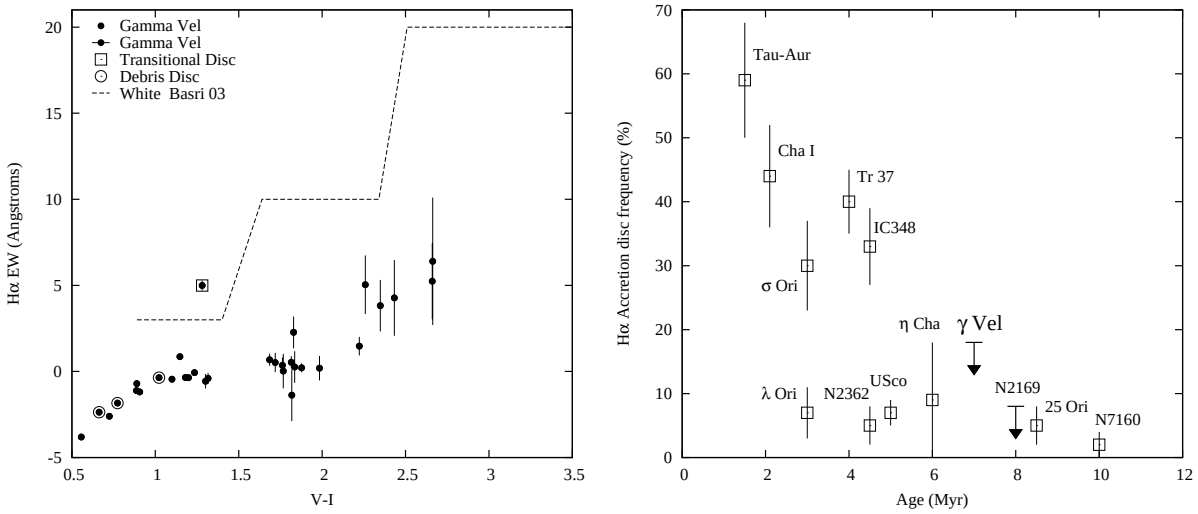

Figure 16. (a) The Hα EWs of spectroscopically confirmed members of the γ Vel association compared with an empirical locus (defined by White & Basri 2003) that separates accreting CTTS from non-accreting WTTS. Also indicated are several stars with indications of circumstellar material in Spitzer near- and mid-IR observations by Hernández et al. (2008). (b) The fraction of low-mass stars ($V-I>1.4$) in the γ Vel association that have accretion signatures (according to the White & Basri [2003] Hα EW criteria) compared with K5-M5 stars in other clusters and associations as a function of age. The data come from Mohanty, Jayawardhana & Basri (2005) for Taurus-Auriga, IC 348, Chamaeleon I and Upper Sco, from Dahm (2005) for NGC 2362, from Sicilia-Aguilar et al. (2005) for Tr 37 and NGC 7160, from Jayawardhana et al. (2006) for the η Cha group, Briceño et al. (2007) for 25 Ori, Jeffries et al. (2007) for NGC 2169 and from Sacco et al. (2008) for σ Ori and λ Ori. The relative precisions for the cluster ages are typically $\pm$1–2 Myr.

be considered a signature of accretion (star ID 16-40, see Fig. 2). This is also the only Hα profile with a width greater than the that accretion threshold of 270 km s^{-1} suggested by White & Basri (2003). All the other objects have Hα EWs consistent with chromospheric emission alone. The stars with debris discs do not show any anomalous behaviour. The low frequency of accreting objects is consistent with the low frequency of class II disc sources found by Hernández et al. (2008).

The disappearance of accretion signatures as young clusters become older is a probe of infalling gas and the evolution of inner discs. Fig. 16b shows the fraction of stars classified as CTTS using the White & Basri (2003) criteria as a function of age for a number of young star forming regions and clusters. In all cases the samples have been restricted to stars with spectral type between K5 and M5 ($V-I>1.4$ in the γ Vel association). The cluster ages are from Mayne & Naylor (2008) where available or we have chosen published ages based on the Siess et al. (2000) isochrones – which are the most consistent with Mayne & Naylor's empirical age scale.

The 95 per cent upper limit to the accretion disc frequency in the γ Vel (as diagnosed from the Hα EW) is 18 per cent. There are ample numbers of spectroscopically unobserved candidate members with which to refine this value, but the present result is consistent with the idea that, with rare exceptions, accretion-related Hα emission is absent for stars older than 5 Myr.

4.7 The total mass and mass function of the Gamma Vel association

In section 3.3 319 stars were defined as low-mass photometric PMS candidates with $V<20$ and $V-I>2$. This sample is almost complete ($\sim$ 85 per cent of such stars have unflagged photometry – see section 2.1) and there will be <117 contaminating field stars within this sample if the density of contaminants is similar to our estimate within the *XMM-Newton* field of view (see section 4.1).

If we assume a distance modulus of 7.76 mag, an extinction of 0.131 mag and an age of 7 Myr, the models of Siess et al. (2000) translate the boundaries of this photometric selection to an approximate mass range of $0.1<M/M_{\odot}<0.6$, with little change for reasonable variations in these assumptions. Correcting for incompleteness, we can say there are between 238–375 stars in this mass range for the area covered by our photometric survey. Poissonian uncertainties are negligible compared with uncertainty in the contamination fraction. If we assume the "universal" mass function advocated by Kroupa (2001) ($\psi(M)\propto M^{-2.3}$ for $M\geqslant 0.5\,M_{\odot}$ and $\psi(M)\propto M^{-1.3}$ for $0.08<M/M_{\odot}<0.5$), then we expect to see 9–14 higher mass stars with $1.8<M/M_{\odot}<4.4$, corresponding to $7<V_T<10$ at the distance/extinction of the association, according to the solar metallicity models of Lejeune & Schaerer (2001). Consulting Fig. 7, there are actually 22 stars on the main sequence in this range, 14 of which are within our photometric survey area, though we cannot be absolutely sure that all of these are association members. Hence the observed ratio of high- to low-mass stars is consistent with the assumed mass function.

We can go a step further and ask how likely it is to find stars as massive as γ^1 Vel and γ^2 Vel in this association? γ^1 Vel is 14 $M_{\odot}$ and the O-star component of γ^2 Vel is 28.5 $M_{\odot}$. The WC component is presently less massive than the O-star, but was $>40\,M_{\odot}$ in the past (see section 4.5). The number of stars more massive than 10 $M_{\odot}$ predicted by the Kroupa mass function is 1.4–2.1, whilst the number with $M>40\,M_{\odot}$ is expected to be only 0.1–0.2. Of course

these predictions assume that all the association low-mass stars have been found, but we know (see section 4.1) that our survey has not yet reached the spatial boundary of this young aggregate, so these predicted numbers are lower limits. We conclude that although the relative numbers of low- and high-mass stars is as expected for a Kroupa (2001) mass function, the presence of a system as massive as γ^2 Vel may be unexpected.

The total mass of the association within the photometrically surveyed area can be estimated by integrating the Kroupa mass function (normalised to the low-mass candidates) up to $10\,M_{\odot}$ and then adding the masses of γ^1 and γ^2 Vel (for which membership is certain by definition!). We apply an approximate correction factor of 1.25 to the integrated mass function to account for the likelihood that about half of the stars in our mass function will be in binary systems with a roughly flat mass-ratio distribution (see Jeffries et al. 2004). The total mass is is 250–360 $M_{\odot}$ depending on how much contamination is present among the low-mass photometric candidates. If the additional high-mass stars found within a 45 arc-minute radius, but outside our photometrically surveyed area are also association members, and stars of different masses are spatially distributed in the same way, then the total association mass could rise to 360–530 $M_{\odot}$. Of course at present there is no way of knowing where the cluster around γ Vel ends and the Vela OB2 association begins, so a better question might be what is the total mass of the Vela OB2 association if a Kroupa-like mass function is widely applicable?

There are 74 objects selected as Vela OB2 members by de Zeeuw et al. (1999), which lie close to the proposed main sequence and have $4 < V < 9$, a range where the Hipparcos catalogue should be almost complete. This magnitude range corresponds to $2.5 < M/M_{\odot} < 17$ according to the solar metallicity models of Lejeune & Schaerer (2001). Extrapolating to $0.1\,M_{\odot}$ using the Kroupa mass function, we would expect to find a further ~ 2300 association members with $9 < V < 20$ and a total association mass of $\sim 1700\,M_{\odot}$.

5 DISCUSSION

In this paper we have established that there is a large group of very young, low-mass stars in the direction of γ Vel which are both spatially and kinematically coherent. The question is how are these stars related to γ Vel and the wider Vela OB2 association? This relationship can be probed in terms of distance, kinematics and age.

In sections 4.2 and 4.3 we found that the distance to the Vela OB2 association (7.72 ± 0.08) and the distance to MS stars around γ Vel (7.76 ± 0.07) agree with good precision. These distances also fall between the two interferometric distances to γ^2 Vel ($7.82^{+0.22}_{-0.07}$ – Millour et al. 2007; 7.63 ± 0.05 – North et al. 2007). In section 4.7 we showed that the numbers of low- and high-mass stars around γ Vel are in a ratio that is consistent with a typical cluster or field star mass function.

The simplest explanations for these observations are that the MS stars around γ Vel are the high mass population commensurate with the low-mass PMS stars we have discovered, that γ^2 Vel is at a similar distance to these stars and that they are all part of the Vela OB2 association. Support for this hypothesis is provided by the significant concentration of low-mass stars around γ Vel (see Fig. 9) and the very similar proper motions of γ^2 Vel, the MS stars around γ Vel, the spectroscopically confirmed low-mass association members and the Hipparcos-selected Vela OB2 members (see 4.1).

There are two potential problems with this model. Firstly, that a very massive object like γ^2 Vel is unlikely to have formed in a cluster consisting of only the stars we have currently identified as γ Vel association members. Weidner & Kroupa (2006) present a simulation (their Fig. 11) aimed at predicting the mass of the most massive star in a cluster of total mass $355\,M_{\odot}$, which is similar to the mass of the γ Vel association within the area of our photometric survey (see section 4.7). For their favoured "sorted-sampling" scenario, the most probable most massive star is $M \simeq 15\,M_{\odot}$, with only a few per cent chance of producing a star as large as the $\geqslant 40\,M_{\odot}$ initial mass of the WC8 star in γ^2 Vel. Secondly, the age of γ^2 Vel is well constrained from its evolutionary status and seems to be significantly less (3–4 Myr) than the age of the low-mass PMS stars (5–10 Myr), although these ages are dependent on the accuracy of evolutionary models in quite different mass ranges.

Rather than problems, these two issues may be important clues to the formation and history of the γ Vel association and its relationship with Vela OB2. Weidner & Kroupa (2006) propose a scenario whereby clusters form in an ordered fashion: the low-mass stars form first and as molecular cloud contraction proceeds, larger amplitude density fluctuations are generated which then form massive stars. This ordering may be enhanced by the build up of the most massive stars through competitive accretion or mergers (Bonnell & Bate 2005, 2006). Once one or more massive stars form near the centre of a cluster then radiative feedback and winds can become important, with the potential to deposit significantly more energy into the intracluster medium than the gravitational binding energy. This could drive out the remaining gas and unbind the cluster (if it were bound to begin with). That the most massive stars in a cluster form after the bulk of low-mass star formation is complete has also been proposed to simultaneously explain why most low-mass stars in the Orion Nebula cluster possess optically thick inner discs, yet there are many "proplyd" objects close to the central massive Trapezium stars with photoevaporation timescales as short as 0.1 Myr (Smith et al. 2005; Clarke 2007)

A possible scenario for the formation of the γ Vel association is as follows. Star formation began about 5–7 Myr ago, with a cluster of low-mass stars forming first. After 1–2 Myr the γ^2 Vel system formed and the Lyman continuum flux from the $\geqslant 40\,M_{\odot}$ WC8 progenitor and the O-star component ($\leqslant$O5V+O7.5V, $\geqslant 3 \times 10^{49}$ ionising photons s^{-1} – Martins, Schaerer & Hillier 2005) could rapidly ionise and drive out the remaining gas, terminating star formation in its vicinity. At this stage most of the cluster mass is in the form of gas, so its expulsion is likely to unbind the cluster (e.g. Weidner et al. 2007). The present kinematic data offer only an upper limit of $\sim 2\,\mathrm{km\,s^{-1}}$ on the 1-dimensional velocity dispersion of association members, but the escape velocity for stars in our photometric survey is only $\simeq 0.5\,\mathrm{km\,s^{-1}}$. Unbound association members would then drift for about 3 Myr and during this time the association could expand

from an initially compact configuration to a diameter of 6–12 pc, corresponding to 1–2 degrees on the sky. It is quite possible that much of the initial stellar population of the association now lies outside the 1 degree field of our photometric survey (as suggested in section 4.1) and that the total initial stellar mass could be closer to the $\sim 1000\,M_{\odot}$ that Weidner & Kroupa (2006) suggest should be associated with the formation of a $40\,M_{\odot}$ star. A wider photometric survey could confirm this suggestion and may find the "edge" of the distribution of low-mass stars associated with γ Vel.

The scenario described above does not account for the rest of Vela OB2, which evidences recent star formation over a diameter that is 5 times larger. Most of these other early-type stars cannot have been in a more compact configuration within the γ Vel association, because there has been insufficient time for them to travel to their present positions. In section 4.7 we found that the γ Vel association we have observed contains 15–20 per cent of the anticipated low-mass stars (and total mass) of the Vela OB2 association (providing the mass function is spatially constant), but this fraction is found within only ~ 1 per cent of the area covered by Vela OB2. This indeed suggests that the γ Vel association is a subcluster within the Vela OB2 assocation and is supported by the clustering of the low-mass stars around γ Vel shown in Fig. 9.

On the other hand, the coherence of their proper motions suggests that all these stars did at least form in the same molecular cloud. There are at least two possible explanations: (1) Star formation was triggered across the cloud, perhaps by some external event like a nearby supernova (in the older, but nearby Trumpler 10 cluster for example – de Zeeuw et al. 1999). Star formation then proceeds as described by the hydrodynamic simulations of Clark et al. (2005), with the development of a number of spatially distinct, close-to-coeval subclusters, which become unbound and disperse as they form more massive stars. (2) Star formation could progress in a sequential manner, with the expanding H II region of an initial generation of high-mass stars compressing the surrounding molecular material, triggering new bursts of star formation (e.g. Dale, Bonnell & Whitworth 2007).

A very wide photometric survey of the Vela OB2 association should be capable of distinguishing between these scenarios, using low-mass PMS stars as age probes. In the first model, the PMS stars will show little or no spatial concentration around the early-type stars (at least no more than we have found around γ Vel) and should have only small, spatially incoherent age variations. In the second model we would expect to find distinct age gradients (becoming younger radially outwards from γ Vel if it marks where star formation commenced), with younger PMS stars being more closely clustered around their high-mass siblings.

Throughout this paper we have assumed that γ Vel and its association have a roughly solar metallicity. It is worth investigating (prompted by the referee) what might happen to the scenario discussed above if this assumption is relaxed. (1) If we assume that the metallicity is roughly half-solar, the main-sequence fitting distance moduli would decrease by ~ 0.4 mag, but the estimated reddening would remain approximately unchanged (Mayne & Naylor 2008). This would place the main-sequence stars around γ Vel and the stars of Vela OB2 in front of the interferometric distances to γ Vel by ~ 0.3 mag, casting doubt on the association of γ Vel with the surrounding main-sequence and PMS stars. A twice-solar metallicity would increase the main-sequence fitting distances leading to better agreement with the mean Hipparcos parallax of Vela OB2 (de Zeeuw et al. 1999) but even worse agreement with the distance to γ Vel. (2) The $Z = 0.01$ low-mass isochrones of Siess et al. (2000) are intrinsically about 0.25 mag fainter than the Z=0.02 isochrones. However, taking into account the ~ 0.4 mag decrease in the distance modulus we would get a slightly older age from modelling the PMS in the CMD. The empirical cluster comparison would only be affected by the distance modulus change and Fig. 15a shows that a 0.4 mag decrease in distance modulus would lead to the γ Vel PMS being significantly older than 25 Ori. A twice-solar metallicity would yield an age more similar to Sigma/Lambda Ori. (3) Meynet et al. (1994) and Meynet & Maeder (2005) consider the evolution of very high-mass stars of differing metallicity. A half-solar metallicity would increase the deduced age and mass of the O-star component of γ Vel to 4.5 Myr and $34\,M_{\odot}$. A half-solar metallicity progenitor to the WC8 component would have to be more massive than $60\,M_{\odot}$ to avoid a red supergiant phase and the total stellar lifetime still less than 5 Myr.

In summary a lower metallicity could increase the age of γ Vel but at the expense of also significantly increasing the deduced age for the low-mass PMS. A twice-solar metallicity could bring the ages of the PMS and γ Vel into agreement and also yield a distance for the main-sequence around $\gamma\,Vel$ that is similar to the Hipparcos distance to Vela OB2. However in either the low or high-metallicity scenarios there would be a very significant disagreement between the interferometric distance to γ^2 Vel and the main sequence fit to the bright stars around it. From the evidence provided by the spatial and kinematic coherency of γ Vel and its surrounding association we do not consider either possibility likely.

6 SUMMARY

The main findings of this paper can be summarised as follows:

- We have extended the survey of Pozzo et al. (2000) and photometrically identified a group of several hundred low-mass PMS stars surrounding the high-mass spectroscopic binary system γ^2 Vel and its early-type common proper-motion companion γ^1 Vel (which together we refer to as the γ Vel system). The youth of a subsample of these objects has been qualitatively confirmed by the presence of lithium in their atmospheres, Hα emission and high levels of X-ray activity.
- The spectroscopically confirmed PMS stars show coherence in their radial velocities and proper motions. They share a common proper motion with γ Vel, a sample of high-mass stars in the vicinity of γ Vel and the Vela OB2 association. There is evidence for a spatial concentration of the PMS stars around γ Vel, but also evidence that the "edge" of this association has not been reached in our 0.9 square degree survey.
- The number of higher mass main-sequence stars surrounding γ Vel is commensurate with the number of lower

mass PMS stars in the region according to the Kroupa (2001) "universal" mass function. The total mass of the association within our surveyed area is 250–360 $M_{\odot}$. The intrinsic distance modulus of the higher mass stars, determined by main-sequence fitting, is 7.76 ± 0.07 mag. This agrees well with a similarly-determined distance modulus of 7.72 ± 0.08 mag for the Vela OB2 association as a whole and is also in accord with interferometric distance determinations to γ^2 Vel. There now seems little doubt that the low-mass PMS stars are associated with γ Vel and that these are all part of the Vela OB2 association.

- The age of γ^2 Vel is well constrained by current high-mass stellar models to be less than 5 Myr and more likely 3–4 Myr. Fitting low-mass isochrones to the PMS population suggests much older ages ($\simeq$ 10 Myr) and empirically placing the PMS stars in an age sequence with other well-studied young clusters on the basis of their position in the Hertzsprung-Russell diagram and lithium depletion suggests ages of 5–10 Myr.
- Accretion activity, as judged by the levels of Hα emission has almost entirely ceased in the PMS stars. The only example of an accretor when defined in this manner has been previously identified as possessing a "transitional" disc on the basis of its infra-red colours.
- We can speculate that γ^2 Vel was formed after the bulk of the low-mass population and its ionising radiation may have been responsible for driving out gas, terminating star formation and unbinding the "γ Vel association". The low observed velocity dispersion of the PMS population suggests that the whole Vela OB2 association cannot have originated close to γ^2 Vel. The concentration of stars and stellar mass close to γ Vel also suggests that it is a subcluster within Vela OB2. Star formation in Vela OB2 must have begun at several sites within the same molecular cloud, either sequentially, resulting in measurable age gradients or perhaps as a result of an external trigger, in which case PMS populations across Vela OB2 may be coeval.

ACKNOWLEDGMENTS

This work is based upon optical observations collected at the Blanco and 0.9-m telescopes of the Cerro Tololo Interamerican Observatory and X-ray observations collected by the *XMM-Newton* satellite and analysed by the *XMM-Newton* Serendipitous Source Catalogue consortium led by the University of Leicester.

Sadly, Christina (Tina) Devey died before the completion of this work and this paper is dedicated to her memory.

We thank the referee (Sofia Randich) for a very careful examination of the manuscript.

REFERENCES

Baraffe I., Chabrier G., Allard F., Hauschildt P. H., 1998, A&A, 337, 403
Baraffe I., Chabrier G., Allard F., Hauschildt P. H., 2002, A&A, 382, 563
Bessell M. S., 2000, PASP, 112, 961
Bessell M. S., Castelli F., Plez B., 1998, A&A, 333, 231
Bohlin R. C., Savage B. D., Drake J. F., 1978, ApJ, 224, 132
Bonnell I. A., Bate M. R., 2005, MNRAS, 362, 915
Bonnell I. A., Bate M. R., 2006, MNRAS, 370, 488
Briceño C., Hartmann L., Hernández J., Calvet N., Vivas A. K., Furesz G., Szentgyorgyi A., 2007, ApJ, 661, 1119
Burningham B., Naylor T., Jeffries R. D., Devey C. R., 2003, MNRAS, 346, 1143
Clark P. C., Bonnell I. A., Zinnecker H., Bate M. R., 2005, MNRAS, 359, 809
Clarke C. J., 2007, MNRAS, 376, 1350
Cutri, R. M. et al. 2003, Technical report, Explanatory supplement to the 2MASS All Sky data release. http://www.ipac.caltech.edu/2mass/
Dahm S. E., 2005, AJ, 130, 1805
Dale J. E., Bonnell I. A., Whitworth A. P., 2007, MNRAS, 375, 1291
D'Antona F., Mazzitelli I., 1997, Mem. Soc. Astr. It., 68, 807
de Zeeuw P. T., Hoogerwerf R., de Bruijne J. H. J., Brown A. G. A., Blaauw A., 1999, AJ, 117, 354
Hernández C. A., Sahade J., 1980, PASP, 92, 819
Hernández J., Hartmann L., Calvet N., Jeffries R. D., Gutermuth R., Muzerolle J., Stauffer J., 2008, ApJ, 686, 1195
Høg E., Fabricius C., Makarov V. V., Urban S., Corbin T., Wycoff G., Bastian U., Schwekendiek P., Wicenec A., 2000, A&A, 355, L27
Jayawardhana R., Coffey J., Scholz A., Brandeker A., van Kerkwijk M. H., 2006, Astrophys. J. , 648, 1206
Jeffries R. D., 2006, in Randich S., Pasquini L., eds, Chemical Abundances and Mixing in Stars in the Milky Way and its Satellites Springer-Verlag, Berlin, p. 163
Jeffries R. D., Naylor T., Devey C. R., Totten E. J., 2004, MNRAS, 351, 1401
Jeffries R. D., Oliveira J. M., Barrado y Navascués D., Stauffer J. R., 2003, MNRAS, 343, 1271
Jeffries R. D., Oliveira J. M., Naylor T., Mayne N. J., Littlefair S. P., 2007, MNRAS, 376, 580
Kenyon S. J., Hartmann L. W., 1995, ApJS, 101, 117
Kroupa P., 2001, MNRAS, 322, 231
Landolt A., 1992, AJ, 104, 340
Lejeune T., Schaerer D., 2001, A&A, 366, 538
Martins F., Schaerer D., Hillier D. J., 2005, A&A, 436, 1049
Mayne N. J., Naylor T., 2008, MNRAS, 386, 261
Mayne N. J., Naylor T., Littlefair S. P., Saunders E. S., Jeffries R. D., 2007, MNRAS, 375, 1220
Meynet G., Maeder A., 2003, A&A, 404, 975
Meynet G., Maeder A., 2005, A&A, 429, 581
Meynet G., Maeder A., Schaller G., Schaerer D., Charbonnel C., 1994, A&AS, 103, 97
Millour, F. et al. 2007, A&A, 464, 107
Mohanty S., Jayawardhana R., Basri G., 2005, ApJ, 626, 498
Naylor T., 1998, MNRAS, 296, 339
Naylor T., Jeffries R. D., 2006, MNRAS, 373, 1251
Naylor T., Totten E. J., Jeffries R. D., Pozzo M., Devey C. R., Thompson S. A., 2002, MNRAS, 335, 291
North J. R., Tuthill P. G., Tango W. J., Davis J., 2007, MNRAS, 377, 415
Pinsonneault M. H., Stauffer J. R., Soderblom D. R., King J. R., Hanson R. B., 1998, ApJ, 504, 170

Pozzo M., Jeffries R. D., Naylor T., Totten E. J., Harmer S., Kenyon M., 2000, MNRAS, 313, L23
Randich S., Aharpour N., Pallavicini R., Prosser C. F., Stauffer J. R., 1997, A&A, 323, 86
Randich S., Pallavicini R., Meola G., Stauffer J. R., Balachandran S., 2001, A&A, 372, 862
Raymond J. C., Smith B. W., 1977, ApJS, 35, 419
Sacco G. G., Franciosini E., Randich S., Pallavicini R., 2008, A&A, 488, 167
Scelsi L., Maggio A., Micela G., Briggs K., Güdel M., 2007, A&A, 473, 589
Schaerer D., Schmutz W., Grenon M., 1997, ApJ, 484, L153
Schmutz W., Schweickhardt J., Stahl O., Wolf B., Dumm T., Gang T., Jankovics I., Kaufer A., Lehmann H., Mandel H., Peitz J., Rivinius T., 1997, A&A, 328, 219
Sicilia-Aguilar A., Hartmann L. W., Hernández J., Briceño C., Calvet N., 2005, AJ, 130, 188
Siess L., Dufour E., Forestini M., 2000, A&A, 358, 593
Smith L. F., 1968, MNRAS, 138, 109
Smith N., Bally J., Shuping R. Y., Morris M., Kassis M., 2005, AJ, 130, 1763
Strüder, L. et al. 2001, A&A, 365, L18
Turner, M. J. L. et al. 2001, A&A, 365, L27
van Leeuwen F., 2007, Hipparcos, the new reduction of the raw data. Springer, Dordrecht
Weidner C., Kroupa P., 2006, MNRAS, 365, 1333
Weidner C., Kroupa P., Nürnberger D. E. A., Sterzik M. F., 2007, MNRAS, 376, 1879
White R. J., Basri G., 2003, ApJ, 582, 1109
Zacharias N., Monet D. G., Levine S. E., Urban S. E., Gaume R., Wycoff G. L., 2004, in Bulletin of the American Astronomical Society Vol. 36 of Bulletin of the American Astronomical Society, The Naval Observatory Merged Astrometric Dataset (NOMAD). pp 1418–+

This paper has been typeset from a TEX/ LATEX file prepared by the author.